RSC Advances

PAPER

View Article Online
View Journal | View Issue

Cite this: *RSC Adv.*, 2026, **16**, 21447

Synthesis, characterization, *in vitro* and *in silico* studies of novel lophine clubbed acylthioureas

Sayyed Aqib Ullah,[a] Hafsa Jabeen,[b] Areeba Javed,[a] Abdul Manan,[a] Nadeem Irshad,[b] Kashif Maqbool Khan,[c] Aneela Khushal,[d] Sara Khan,[de] Umar Farooq,[d] Kashif Bashir *[b] and Aamer Saeed *[a]

In the present study, a chemical library of novel lophine clubbed acylthioureas (**8a–l**) was designed and synthesized through a multistep sequence. 2-(4-Nitrophenyl)-4,5-diphenyl-1*H*-imidazole (**3**) was synthesized from benzil, 4-nitrobenzaldehyde, and ammonium acetate *via* multicomponent reaction. Then the nitro group of the synthesized compound was reduced using zinc and hydrochloric acid to furnish 4-(4,5-diphenyl-1*H*-imidazol-2-yl) aniline (**4**). On the other hand, the acid chloride (**6a–l**) of substituted benzoic acids was prepared by reacting acids (**5a–l**) with thionyl chloride, followed by their reaction with potassium thiocyanate to afford corresponding acyl isothiocyanates (**7a–l**), which were further reacted with 4-(4,5-diphenyl-1*H*-imidazol-2-yl)aniline (**4**) to produce acylthioureas (**8a–l**) in good yield. The synthesized series (**8a–l**) was characterized by using a combination of spectroscopic techniques, including FT-IR, ^{1}H NMR, and ^{13}C NMR. Moreover, the synthesized acylthiourea derivatives were assayed for their *in vitro* and *in silico* xanthine oxidase and thymidine phosphorylase inhibitory activities. In the tested series, compounds **8j**, **8d**, and **8i** showed robust dual inhibition profiles in low micromolar ranges. Among them, compound **8j** revealed the most potent activity, with IC_{50} values of 1.87 ± 0.26 μM against xanthine oxidase and 1.62 ± 0.27 μM against thymidine phosphorylase. Compound **8d** sits in the next position, with an IC_{50} value of 3.34 ± 0.37 μM (xanthine oxidase) and 3.31 ± 0.06 μM (thymidine phosphorylase), while compound **8i** demonstrated considerable xanthine oxidase inhibition with an IC_{50} of 2.06 ± 0.36 μM. These values have outperformed the standard drug allopurinol (IC_{50} = 7.4 ± 0.07 μM), which was found to be less potent against xanthine oxidase. Considering the established involvement of these enzymes in oxidative stress, hyperuricemia, and inflammation-based disorders, the results endorse the idea of these derivatives being promising multifunctional therapeutic agents in the treatment of metabolic, inflammatory, and neoplastic diseases.

Received 15th February 2026
Accepted 9th April 2026

DOI: 10.1039/d6ra01337f

rsc.li/rsc-advances

1 Introduction

In medicinal chemistry, molecular hybridization is an intriguing technique for creating pharmaceuticals with two or more moieties of distinct pharmacological properties.[1] It is feasible to develop hybrid compounds that are more effective by considering the biological behaviors of the moieties. These molecules would have improved binding interactions and inhibitor pocket packing with the receptors. Imidazole is a five-membered planar aromatic ring that contains two nitrogen atoms at positions 1 and 3. $C_3H_4N_2$ is the molecular formula of the simplest imidazole.[2] Imidazole was discovered in the early 1840s, and the name imidazole was coined by Arthur Rudolf Hantzsch in 1887.[3] The name glyoxaline was used before 1887 for the compounds because it was synthesized for the first time by Henrich Debus in 1858 from glyoxal and ammonia.[4]

Research on the synthesis of imidazole-based organic compounds is being carried out due to their diverse applications as agrochemicals, artificial acceptors, medicinal drugs, biomimetic catalysts, man-made materials, supramolecular ligands, and so on.[5–9] Imidazole contains a peptide backbone unit and shows similarity with carboxamide in physicochemical and biological properties; thus, these are considered as bioisosteres of one another and provide metabolic stability against amidases. Imidazole consists of two nitrogen atoms, one acts as an H-bond acceptor, and the other one as a donor, and the same is the case for carboxamide; the only difference is the presence of one oxygen instead of a nitrogen atom.[10,11] Similarly, imidazole is found as an isostere replacement of various 5-membered heterocycles such as thiazole,[12] oxazole,[13] tetrazole,[14] pyrazole,[15] and triazole[16] because all these

[a]*Department of Chemistry, Quaid-i-Azam University, Islamabad 45320, Pakistan. E-mail: asaeed@qau.edu.pk*

[b]*Department of Pharmacy, Quaid-i-Azam University, Islamabad 45320, Pakistan. E-mail: kbashir@qau.edu.pk*

[c]*Institute of Pharmaceutical Sciences, University of Veterinary and Animal Sciences, Lahore 54000, Pakistan*

[d]*Department of Chemistry, COMSATS University Islamabad, Abbottabad Campus, Abbottabad, 22060, Pakistan*

[e]*Department of Chemistry, Pennsylvania State University, University Park, PA, USA*

compounds show similarity in biological and physicochemical properties due to the same valence electronic distribution, and all compounds have the same hydrogen bonding and π–π stacking interactions with biological systems.[17]

2,4,5-Triphenyl-1*H*-imidazole, also called lophine, is an attractive chemiluminescent and fluorescence compound. Radziszewski reported the chemiluminescence properties of lophine for the first time in 1877. He observed that when lophine reacts with oxygen and a strong base, it emits yellow light.[18] Thioureas are organosulfur compounds with the general formula RNHC(S)NHR′ and are similar in structure to urea except for the replacement of the oxygen atom of urea by a sulfur atom; consequently, the chemical characteristics of both are considerably different.[19] Thiourea was synthesized in 1873 by Marceli Nencki as a white solid crystal with a melting point of 176–178 °C for the first time as a urea analog.[20] The reason for extensive research and interest in thioureas is due to their diverse applications, such as plastics,[21] formation of photographic film,[22] and dyes.[23] The derivatives of thiourea have also been reported to have biological applications, such as preservatives,[24] insecticides,[25] and as precursors of pharmaceutical drugs.[26]

Acylthiourea with the general formula (RCONHC(S)NHR′) is obtained by replacing one H atom of NH_2 in thiourea with an acyl group (RC═O), where R may be an aryl, alkyl, aralkyl, or heterocyclic group. Acylthioureas have two coordinating sulfur and nitrogen atoms, thus acting as bidentate ligands and leading to the formation of metal complexes.[27] Extensive research on acyl thiourea was due to its effective, diverse nature of applications in various fields, such as organo-catalysts,[28,29] molecular recognition, pharmaceuticals, agriculture, material science, and biological activities.[30] Some important biological activities include antimicrobial,[31] antidiabetic,[32] herbicidal,[33] fungicidal,[34] antiparasitic,[35] pesticidal,[36] urease inhibition,[37] and anticancer agents.[38] Some biologically active compounds containing imidazole, thiourea, and acylthiourea moieties are shown in Fig. 1.

Keeping in mind the above-mentioned molecular hybridization concept and the wide spectrum of imidazole and

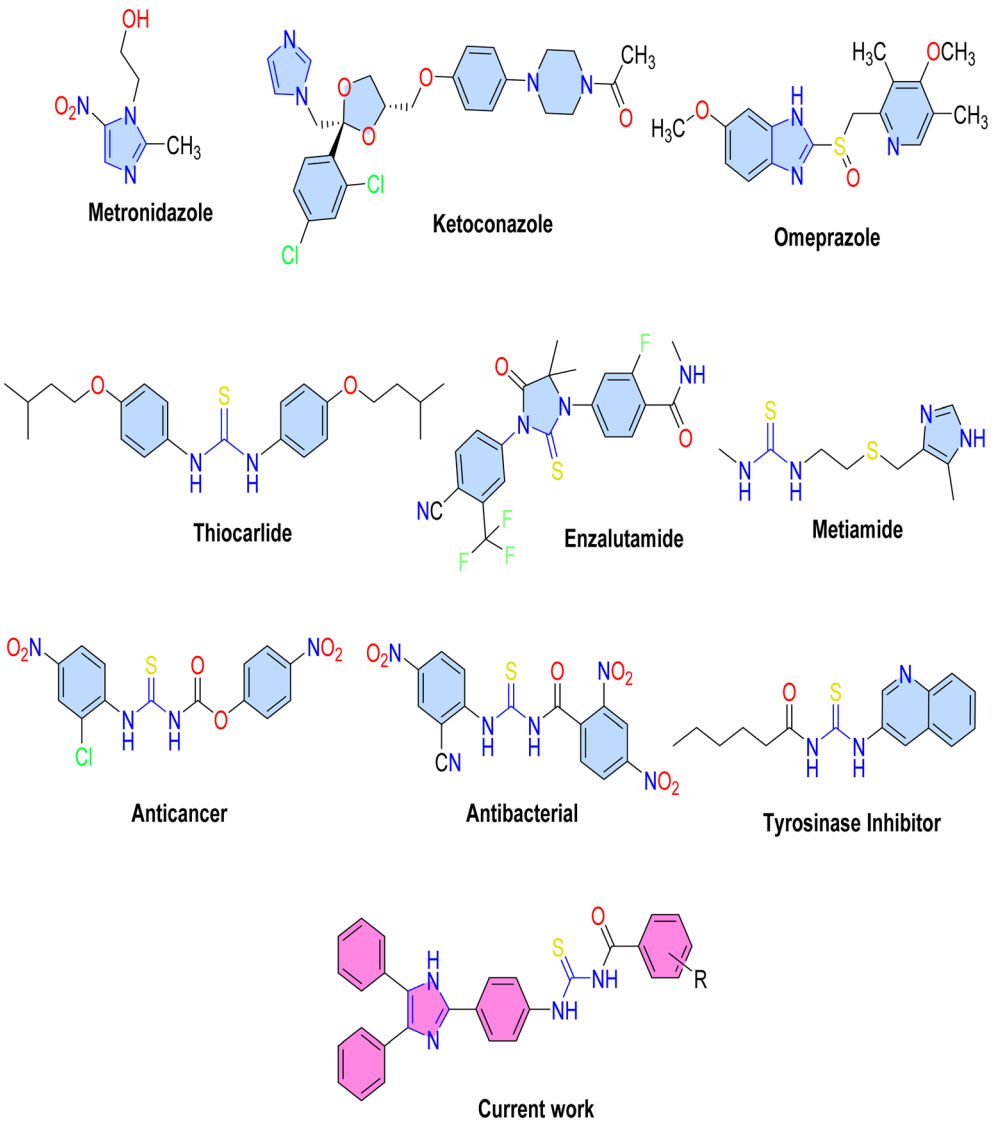

Fig. 1 Previously reported some biologically potent compounds.

acylthioureas activities, herein we report the synthesis of imidazole-linked acylthioureas to enhance effectiveness and broaden the pharmaceutical scope of acylthioureas.

Much attention has been directed in recent years to the therapeutic targeting of enzymes involved in oxidative stress and nucleotide metabolism with respect to inflammation-related metabolic disorders. Of these, xanthine oxidase and thymidine phosphorylase have emerged as clinically relevant enzymes because of their respective roles in purine catabolism and the generation of pro-oxidant metabolites. For example, xanthine oxidase represents a key source of ROS and uric acid, contributing to oxidative damage and gout disease, while thymidine phosphorylase is implicated in the production of 2-deoxy-D-ribose, an agent that evokes inflammation and endothelial dysfunction. Thus, compounds that can inhibit both xanthine oxidase and thymidine phosphorylase may afford therapeutic benefits in the management of diseases such as gout, atherosclerosis, and related disorders driven by oxidative and inflammatory mechanisms.[39,40]

A scaffold of acylthiourea has been considered a privileged pharmacophore in medicinal chemistry, as it can interact with an enzyme active site through hydrogen bonding, metal coordination, and favorable electrostatic interactions. Therefore, this would turn out to be particularly suitable for interacting with the catalytic or cofactor-binding domains of oxidoreductases and phosphorylases.[41,42] Structurally based on this, a series of lophine-conjugated acylthiourea derivatives has been designed to explore their potential for dual inhibition of xanthine oxidase and thymidine phosphorylase enzymes. The biological implication of those substances was further studied by molecular docking and *in vitro* enzyme inhibition studies to probe their binding affinity and functional activity.[39,41]

2 Results and discussions

2.1 Chemistry

A novel class of lophine-linked acyl thiourea derivatives was synthesized *via* a multistep synthesis. These steps include heterocyclization, reduction, nucleophilic substitution, and addition reactions. 2-(4-Nitrophenyl)-4,5-diphenyl-1*H*-imidazole was synthesized from benzil, 4-nitrobenzaldehyde, and ammonium acetate *via* a multicomponent heterocyclization reaction. Then the nitro group of the synthesized compound was reduced using zinc and hydrochloric acid to furnish 4-(4,5-diphenyl-1*H*-imidazol-2-yl) aniline. On the other hand, the acid chloride of substituted benzoic acids was prepared through nucleophilic substitution reaction by reacting acids with thionyl chloride followed by their reaction with potassium thiocyanate to afford corresponding acyl isothiocyanates, which were further reacted with 4-(4,5-diphenyl-1*H*-imidazol-2-yl)aniline to produce acyl thioureas *via* nucleophilic addition reaction (**8a–l**) in good yield as can be seen in Scheme 1.

The structures of all novel synthesized lophine clubbed acylthiourea pharmacophores were confirmed *via* spectroscopic analysis. A representative example (**8d**) is discussed here.

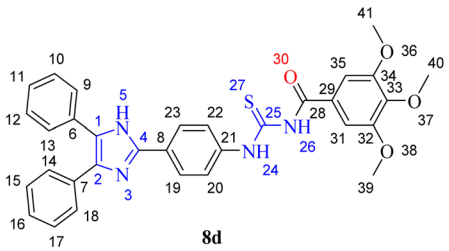

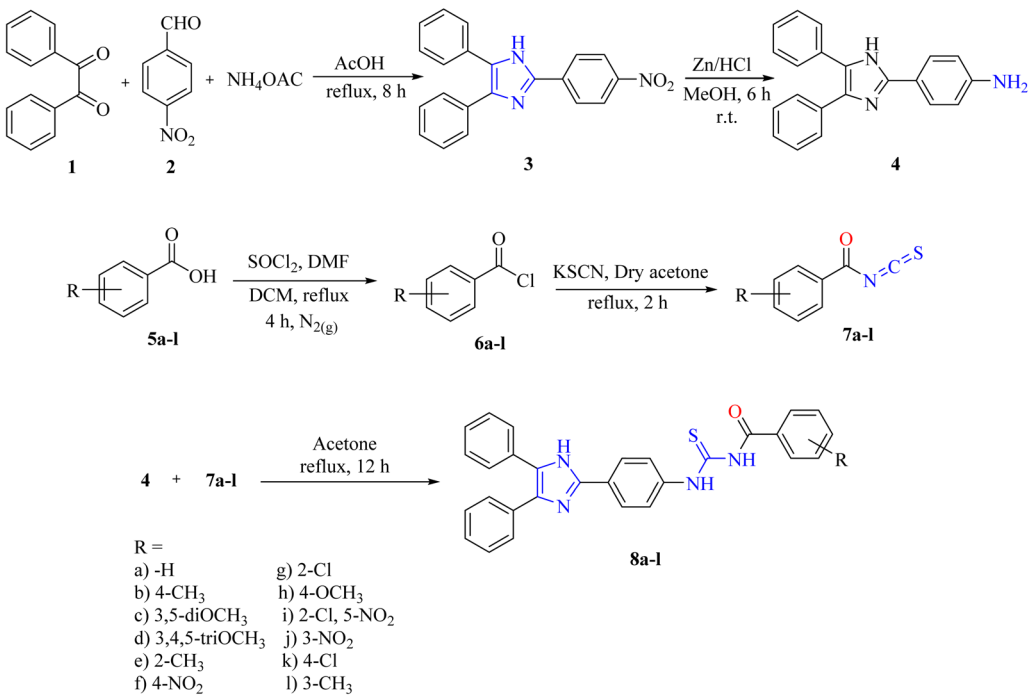

Scheme 1 Synthetic pathway of lophine acylthiourea hybrid pharmacophores.

Synthesized compound **8d** was characterized and confirmed by FT-IR spectroscopy. The stretching bands for Csp^2–H and Csp^3–H bonds were observed at 3031 and 2888 cm^{-1}, respectively. A strong stretch at 1680 cm^{-1} was attributed to the stretching of carbonyl C=O functionality. A stretching band appeared at 1580 cm^{-1} corresponding to the C=C stretching of the aromatic part. Another characteristic stretching band manifested at 1235 cm^{-1} for the C=S bond, further confirming the synthesis of the respective compound. Additionally, there was another strong stretch at 1118 cm^{-1}, indicating the presence of a C–N bond. The presence of sulphur was confirmed by Lassaigne's test.

The characteristic and most deshielded signals at 12.971 and 11.748 ppm appeared as singlets, corresponding to the two NH protons at positions 26 and 24 of the thioamide moiety, which confirmed the synthesis of the respective compound. The proton present at position 26 appeared downfield because of the deshielding effect caused by the carbonyl and thiocarbonyl group attached directly to the nitrogen atom containing the proton. The carbonyl and thiocarbonyl groups here withdraw electrons both inductively and by resonance effect, which makes the proton more deshielded. The signal for the two protons at positions 19 and 23 appeared as doublet at 8.373 ppm with $^3J = 8.7$ Hz by coupling with protons at positions 20 and 22. Signal at 8.057 ppm corresponds to the protons at positions 22 and 24, which appeared as doublet with $^3J = 8.7$ Hz by virtue of coupling with protons at positions 19 and 23. The signal at 8.373 ppm was assigned to the protons at positions 19 and 23 because these protons are *ortho* to the electron-withdrawing imidazole ring, which deshields them through a resonance effect. Signal for four protons at positions 9, 13, 14, and 18 manifested as a multiplet at 7.599–7.569 ppm; these protons appeared slightly deshielded because they are present *ortho* to the electron-withdrawing imidazole ring. Signals for six protons at positions 10, 11, 12, 15, 16, and 17 appeared as a multiplet at 7.521–7.477 ppm. Signals for protons at positions 31 and 35 appeared as a singlet at 7.413 ppm; these protons are slightly shielded compared to the other aromatic protons because of electron-donating methoxy groups, which increase electron density at the *ortho* position through the resonance effect. The most shielded two signals at 3.889 and 3.761 ppm appeared as singlets corresponding to the protons of methoxy groups present at *meta* and *para* positions 39, 41, and 40 of the acylated aromatic part, respectively. pK_a value of the proton at position 5 in the imidazole ring is 14.5, rendering it more acidic than alcohols. Due to this acidity, the signal for the proton does not appear as it can exchange with the solvent.

The most deshielded signals appeared at 179.49 and 167.69 ppm, corresponding to the carbon atoms (28) and (25) of the thiocarbonyl and carbonyl functional groups, respectively, confirming the synthesis of the desired compound. The thiocarbonyl carbon was more deshielded because it relates to three electron-withdrawing electronegative heteroatoms directly. Signals at 153.04 ppm correspond to the carbon of the imidazole ring present between two nitrogen atoms. Carbons (32) and (34) of the aromatic ring, to which the methoxy groups were directly attached, manifested at 143.89 ppm. The signal at 142.13 ppm corresponds to carbon (33) of the aromatic ring to which the methoxy group was directly attached. Signal at 141.28 was assigned to carbon (21) of the aromatic ring. The most shielded signal at 106.79 in the aromatic region was assigned to the carbons (31) and (35) of the aromatic ring present *ortho* to the electron-donating methoxy group, which increases electron density at these positions by the resonance effect. Remaining sp^2 hybridized carbon atoms (1, 2, 8, 9, 10, 11, 12, 13, 14, 15, 16, 17, 18, 19, 20, 22, 23, 29) appeared in the range of 130.04–121.51 ppm. Signals at 60.64 and 56.63 ppm were assigned to the carbon (40) of the methoxy group at the *para* position and carbons (39) and (41) of the methoxy groups at the *meta* position of the aromatic ring, respectively.

2.2 Enzyme inhibition *in silico* studies

Molecular docking was conducted to investigate the interactions of synthesized lophine-based acylthiourea derivatives with xanthine oxidase and thymidine phosphorylase at the molecular level. The co-crystallized ligand was extracted from the protein PDB file and re-docked into the protein using the same parameters to check docking consistency. RMSD values were calculated using the DSV tool, comparing docked *vs.* co-crystallized ligand poses. RMSD values were 1.21 and 1.01 Å, showing significant overlap as shown in Fig. 2. This validates the docking experiment's accuracy.

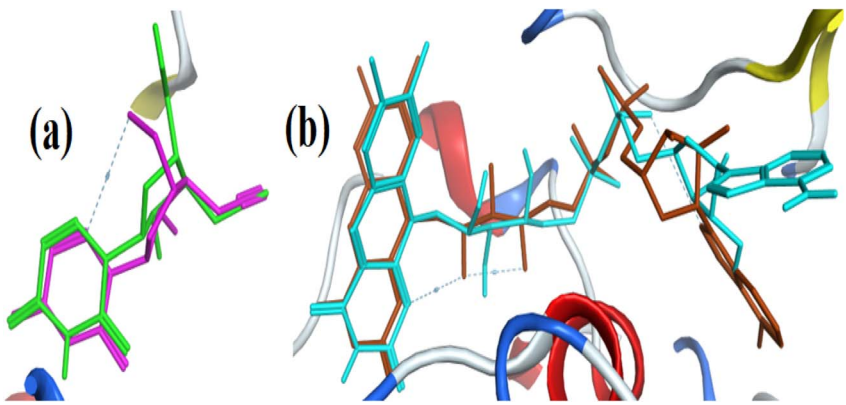

Fig. 2 Re-docking of co-crystallized ligands in the active pockets of selected proteins. (a) Thymidine phosphorylase, and (b) xanthine oxidase.

From molecular docking studies, the binding affinity values revealed that several compounds formed stable complexes with both enzymes. Although the docking scores do not exactly match the IC_{50} values, the docking results still provide useful hints on how the synthesized compounds interact with the enzyme's active sites, including their binding modes and interaction with the enzyme. Among them, compounds **8j** and **8d** exhibited strong binding energies against both targets, while compound **8j** had the most favorable interaction pattern, indicating a good fit within the active sites, which correlated well with its strong enzymatic inhibition observed in the biological assays. Their docking scores were more favorable than those of the reference drugs allopurinol and 7-deazaxanthine, highlighting the potential of such molecules to act as effective dual inhibitors. Such computational results are in good agreement with the experimental enzyme inhibition data, further supporting the therapeutic relevance of the synthesized series. The detailed binding energies of all the compounds are summarized in Table 1.

The docking orientations observed in this study provide insight into the mechanism through which the newly synthesized derivatives might act as inhibitors of the enzymes. From the structural conformation of the enzyme, most inhibitors have been observed to bind within the tight catalytic channel that leads to the molybdenum site, effectively blocking the substrate and preventing the conversion of hypoxanthine to uric acid.[43,44] In this regard, aromatic thiourea derivatives have been observed as competitive or mixed inhibitors that form hydrogen bonds around the catalytic site and hydrophobic stacking interaction within the substrate channel.[44] Previous studies on the molecular docking of small molecule inhibitors have revealed that a number of them bind to residues near the catalytic site and prevent substrate binding at the catalytic site.[45,46] In the current study, the binding of compounds **8j**, **8d**, and **8b** to the catalytic cleft and their interaction through hydrogen bonds to residues such as Ser144, Glu33, and Asp309 suggest a similar mechanism of catalytic site blocking. Such interactions are likely to hold the inhibitor within the gorge of the enzyme and prevent the binding of physiological substrates to the catalytic site containing molybdenum.

Table 1 Docking-based binding energies (kcal mol^{-1}) of synthesized compounds with thymidine phosphorylase and xanthine oxidase

		Binding energy (kcal mol^{-1})	
Sr. #	Code	Xanthine oxidase	Thymidine phosphorylase
1	**8a**	−6.32	−8.31
2	**8b**	−8.23	−6.82
3	**8c**	−6.18	−7.34
4	**8d**	−6.47	−8.50
5	**8e**	−5.84	−7.51
6	**8f**	−7.76	−6.38
7	**8g**	−6.62	−8.22
8	**8h**	−7.47	−7.86
9	**8i**	−5.88	−7.63
10	**8j**	−6.99	−8.43
11	**8k**	−6.11	−6.76
12	**8l**	−8.02	−6.5
13	2b (IMA)	−8.46	−6.90
14	7-Deazaxanthine		−5.62
15	Allopurinol	−5.93	

The observed binding affinities seem to arise from a combination of π–π stacking, dipolar stabilization, and directional hydrogen bonding with both the thiocarbonyl and imidazole nitrogen atoms. This type of interaction is in line with previous studies on acylthiourea-derived heterocycles, in which these key pharmacophoric features are important for effective inhibition of xanthine oxidase and thymidine phosphorylase enzymes.[47,48]

In addition, the extended aromatic system of the lophine core is likely to contribute to the stability of the ligand by forming aromatic–aromatic interactions with the hydrophobic residues in the binding pocket of the enzyme.[49] The compounds **8j** and **8d** can make more effective interactions, and this is probably because substituents, whether electron-withdrawing or electron-donating, alter the electronic properties of the benzamide ring and guide the ligand into a more favorable orientation in the catalytic pocket. Orientation effects are in good agreement with SAR trends obtained in computational analyses of nitro- and methoxy-substituted enzyme inhibitors.[50]

Several important residues in the binding pocket that enable the inhibitor to remain within the active site are revealed by the crystal structure of xanthine oxidase. These consist of two loops with color-coded green and blue residues ranging from 25–52 and 142–153, respectively. Three helices, spanning residues 263–272, 285–308, and 342–345, are also involved in the color-coded yellow, pink, and purple region of the active site. The active site residue of the protein, color-coded brown, black, and orange, include three loops (309–341, 356–361, and 420–436) that are essential for inhibitor binding and retention. Another loop containing residues 1220–1230 also forms part of the cyan-colored region of the active site (Fig. 3).

Docking overlays reveal that the compounds **8d** and **8j**, containing multiple methoxy groups or a *meta*-nitro substituent, orient their substituents toward polar microenvironments within the binding pocket. This action may enhance the ligand–enzyme complex through additional donor–acceptor interactions. The findings were corroborated by Feng *et al.* (2022) in docking studies of methoxy-rich and nitro-substituted phenylthioureas, where substituent-directed orientation influences docking stability.[47] The small discrepancies between the docking results and the experimental IC_{50} values arise from the limitations of the docking scoring function. While the scoring function provides a good estimate of the binding affinity between the ligand and the enzyme, it does not take into consideration the dynamic nature of the enzyme's binding sites.

2.2.1 3D interaction plots of top-ranked compounds. The most potent compounds are characterized by a common binding mode in the catalytic pocket, in which hydrogen bonding with polar residues and hydrophobic or π–π interactions with aromatic amino acids are observed to anchor the ligand in the binding site. The 3D interaction plot of compound **8b** is shown in Fig. 4. The compound **8b** fits into the catalytic pocket, having a binding energy of −8.23 kcal mol^{-1}. Significantly, Ser144 also engages in a strong hydrogen bond with the ligand, increasing binding specificity, whereas Glu33 and

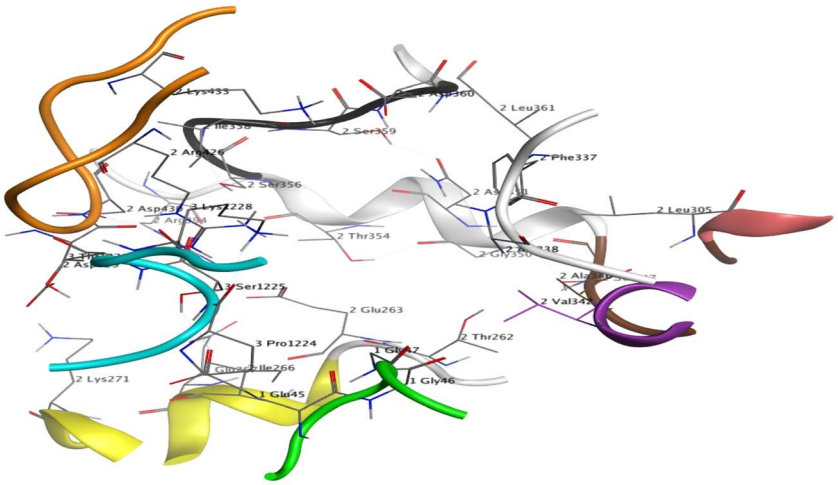

Fig. 3 3D interaction mapping of active site residues of xanthine oxidase.

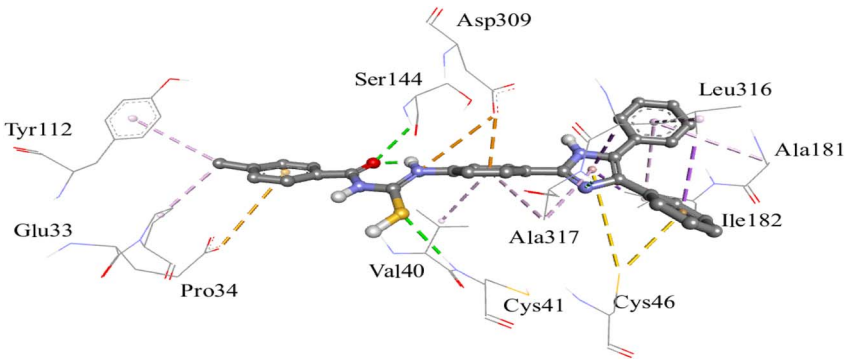

Fig. 4 3D interaction plot of compound **8b**.

Asp309 provide supplementary electrostatic and hydrogen-bonding interactions that secure the molecule in the active site. The cysteine residues with sulfur atoms, Cys41 and Cys46, contribute to the stabilization of the ligand *via* π-sulfur interactions.

Hydrophobic residues such as Ile182, Leu316, Val40, Ala317, and Phe269 form a nonpolar niche that facilitates van der Waals and π–π-alkyl interactions with the ligand's aromatic rings. Collectively, these interactions work together to hold the inhibitor in place in the catalytic cleft of xanthine oxidase. This results in reduced oxidative stress and excessive uric acid production that is mechanistically similar to clinically established xanthine oxidase inhibitors like allopurinol and febuxostat. Indeed, similar binding motifs have been described for other aromatic thiourea inhibitors, which display a remarkable increase in affinity upon hydrophobic enclosure of the aromatic system, combined with anchoring *via* the thiocarbonyl unit in a polar fashion.[48] This mechanistic pattern forms the basis for the combined influence of electronic density and substituent polarity in controlling strong xanthine oxidase binding.

Thymidine phosphorylase forms an S-shaped dimer made up of two subunits when it is co-crystallized with 3-azido-2-fluoro-dideoxyuridine (ONP), according to a thorough structural analysis. The active site is located at the interface between the larger α/β domain and the smaller α-helical domain that make up each subunit. Arg-171, Ser-186, and Lys-190 are important residues that are probably involved in ligand binding. Furthermore, residues 115–123 and 206–212 compose the hydrophobic area of the active site, as shown in Fig. 5.

Docking analyses further indicate that the lophine core complex significantly stabilizes thymidine phosphorylase *via* π–π stacking interactions with aromatic residues, including Tyr168 and His85. These residues have been identified as key contributors to the binding of both nucleoside analogues and non-nucleoside inhibitors.[47] The acylthiourea moiety appears to stabilize this orientation by acting as a polar hinge, enabling the benzamide substituent to align suitably with the catalytic region. This dual anchoring has been reported in structure–activity relationship studies of thiourea- and urea-based thymidine phosphorylase inhibitors, wherein the concurrent presence of an aromatic head group and polar linker markedly enhances binding.[51]

The 3D interaction plot of compound **8a**, shown in Fig. 6, illustrates its positioning within the catalytic pocket of thymidine phosphorylase and highlights the key amino acids

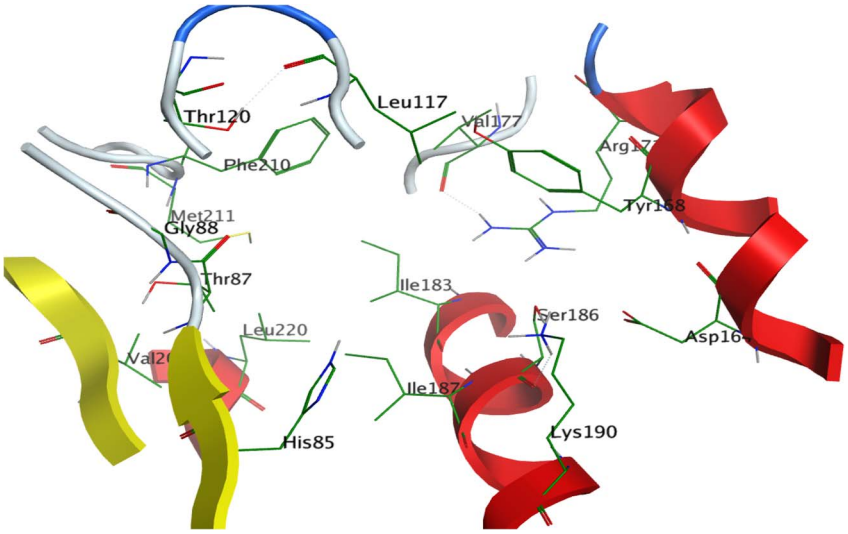

Fig. 5 Active site of thymidine phosphorylase showing key binding residues.

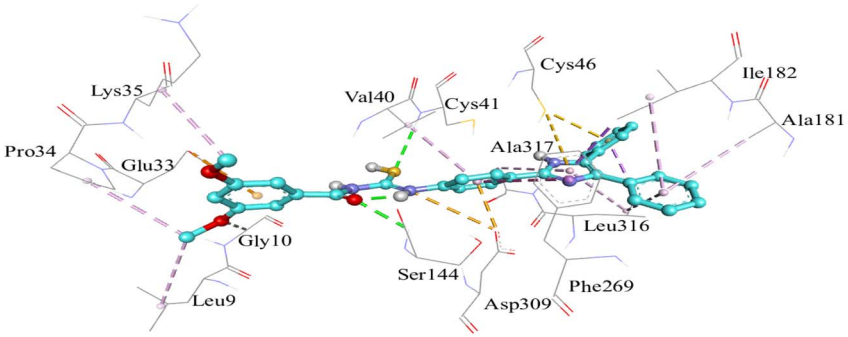

Fig. 6 3D interaction plot of compound **8a**.

involved in ligand recognition. The enzyme catalyzes the reversible phosphorolysis of thymidine to thymine and 2-deoxy-D-ribose-1-phosphate and plays a role in tumor angiogenesis. Multiple hydrogen bonds (green dashed lines) are established with residues like Lys84, Ser95, Thr128, and Gly121, which assist in the orientation of ligand binding. Ionic interactions (orange dashed lines) with residues like Asp92 and Lys130 also reinforce the binding by complementing the charged groups of the ligand. Moreover, hydrophobic and aromatic interactions (pink and purple dashed lines) with residues such as His85, Met111, Leu117, and Tyr168 further underscore the positioning of the ligand **8a** in the binding site by π–π stacking and van der Waals contacts. These interactions facilitate the binding of compound **8a** to the thymidine phosphorylase catalytic pocket.

The pronounced accommodation of compound **8a** within thymidine phosphorylase, despite the absence of electron-withdrawing or electron-donating substituents on the terminal phenyl ring, aligns with recent thymidine phosphorylase inhibitor studies. These studies indicate that planar aromatic systems can interact effectively through π–π stacking and hydrophobic complementarity within the enzyme active site.[52] The current docking results indicate that the lophine–acylthiourea scaffold alone provides sufficient electronic and steric complementarity to offset the lack of benzamide substituents, enabling compound **8a** to capitalize on the same stacking and hydrophobic interactions documented for other aromatic thymidine phosphorylase inhibitor chemotypes.[53]

The 3D interaction plot of compound **8j** is shown in Fig. 7. The compound **8j** is involved in a complicated hydrogen bonding, electrostatic, and hydrophobic network of interactions with some catalytically and structurally significant residues of thymidine phosphorylase. Interestingly, hydrogen bonds (green dashed lines) are noted between compound **8j** and residues Gln156, Lys190, and Ile183, contributing to directional polar interactions with the catalytic residues. Electrostatic interactions (orange and red dashed lines) with Asp164 reflect strong ionic contact and charge complementarity between the negatively charged carboxylate group of Asp164 and the positively polarized areas of the ligand. This contact probably plays a central role in stabilizing the orientation of compound **8j** in the catalytic pocket. In addition, π–π stacking and hydrophobic interactions (pink dashed lines) with His85, Tyr168, and Met111 aid nonpolar stabilization and aromatic ring stacking, which are vital for compound **8j** accommodation in the enzyme's

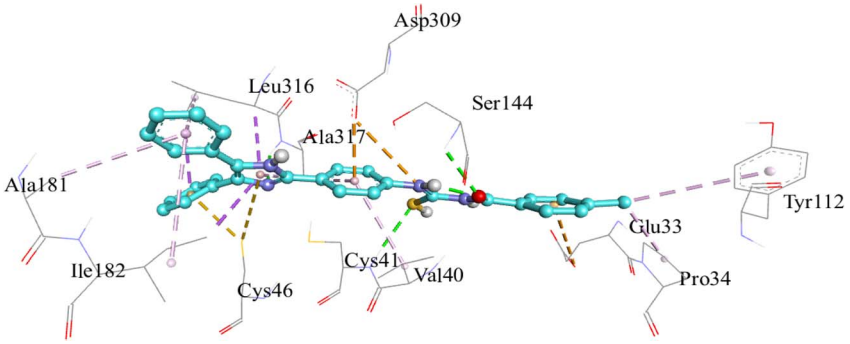

Fig. 7 3D interaction plot of compound **8j**.

hydrophobic channel. Further interactions with amino acids such as Ser113 and Gly114 facilitate the proper positioning of the ligand.

The binding profile of compound **8j** is in good agreement with previously reported docking results for nitro-substituted phenyl inhibitors of thymidine phosphorylase, where the nitro group supports high-affinity binding by orienting its oxygen atoms toward basic residues and thus forming a stable dipolar anchor within the active site.[47] Specifically, the *meta* placement of the nitro group has been shown to preserve aromatic planarity while allowing for favorable hydrogen-bond geometry, thus providing a rationale for the observed marked stability of compound **8j** in the current docking simulations.

2.3 Enzyme inhibition *in vitro* studies

The xanthine oxidase and thymidine phosphorylase inhibition activities of the synthesized compounds are summarized in Table 2. The enzyme concentration used for the inhibition activity was 2 mg ml^{-1}. GraphPad Prism software was used to determine the IC_{50} values at various concentrations.

Nine compounds showed the strongest inhibition against xanthine oxidase and thymidine phosphorylase. The rest of the compounds are also moderate to good inhibitors of both enzymes. Among the synthesized derivatives, compound **8j** was the most potent dual inhibitor, with IC_{50} values of 1.87 μM for xanthine oxidase and 1.62 μM for thymidine phosphorylase.

It was also found that compound **8d** exhibited high potency against both enzymes, whereas compound **8i** demonstrated selective and strong inhibition of xanthine oxidase. This was further supported by the dose–response inhibition curves, in which compounds such as **8j** and **8i** exhibited a sharp, concentration-dependent decrease in absorbance, confirming their potent inhibition of xanthine oxidase. These sigmoidal inhibition trends, plotted through nonlinear regression as shown in Fig. 8, illustrate the effectiveness of these molecules in suppressing enzymatic activity at micromolar levels.

Notably, compound **8j** inhibited thymidine phosphorylase at 88.5%, while **8d** achieved a similar magnitude of activity at 89.3%, demonstrating its strong dual-target activity. In corroboration, inhibition graphs for thymidine phosphorylase in Fig. 9 indicated steep inhibition curves for compounds **8j**, **8d**, and **8i**, which are consistent with their higher percentage inhibition values.

The concentration-response behaviour reflected in these plots provides further experimental evidence of their efficiency

Table 2 Xanthine oxidase and thymidine phosphorylase inhibition activity of synthesized compounds[a]

Sr. #	Compound	% inhibition ± STD (xanthine oxidase)	IC_{50} (μM) ± SEM	% inhibition ± STD (thymidine phosphorylase)	IC_{50} (μM) ± SEM
1	**8a**	67.5 ± 1.16	6.18 ± 1.04	83.5 ± 1.16	4.17 ± 0.03
2	**8b**	53.8 ± 1.09	410.00 ± 1.18	49.8 ± 1.09	_
3	**8c**	84.6 ± 1.01	2.64 ± 0.19	44.6 ± 1.01	_
4	**8d**	81.3 ± 0.91	3.34 ± 0.37	89.3 ± 0.91	3.31 ± 0.06
5	**8e**	70.0 ± 1.23	4.40 ± 0.30	37.0 ± 1.23	_
6	**8f**	41.1 ± 2.14	_	65.1 ± 2.14	4.39 ± 0.21
7	**8g**	46.3 ± 1.12	_	39.3 ± 1.12	_
8	**8h**	51.3 ± 0.89	482.00 ± 1.01	52.3 ± 0.89	452.00 ± 0.94
9	**8i**	83.8 ± 1.23	2.06 ± 0.36	33.8 ± 1.23	_
10	**8j**	87.5 ± 1.67	1.87 ± 0.26	88.5 ± 1.67	1.62 ± 0.27
11	**8k**	50.0 ± 1.86	500.00 ± 0.84	55.5 ± 1.92	393.00 ± 1.16
12	**8l**	65.5 ± 1.92	4.73 ± 0.29	81.0 ± 1.86	2.96 ± 0.14
13	2b (IMA)	60.8 ± 1.15	6.23 ± 0.17	54.0 ± 1.15	372.00 ± 0.92
14	7-deazaxanthine			89.0 ± 1.63	41.00 ± 0.24
15	Allopurinol	86.5 ± 1.37	7.40 ± 0.07		

[a] The IC_{50} values were obtained only for those compounds that achieved at least 50% inhibition at a particular concentration.

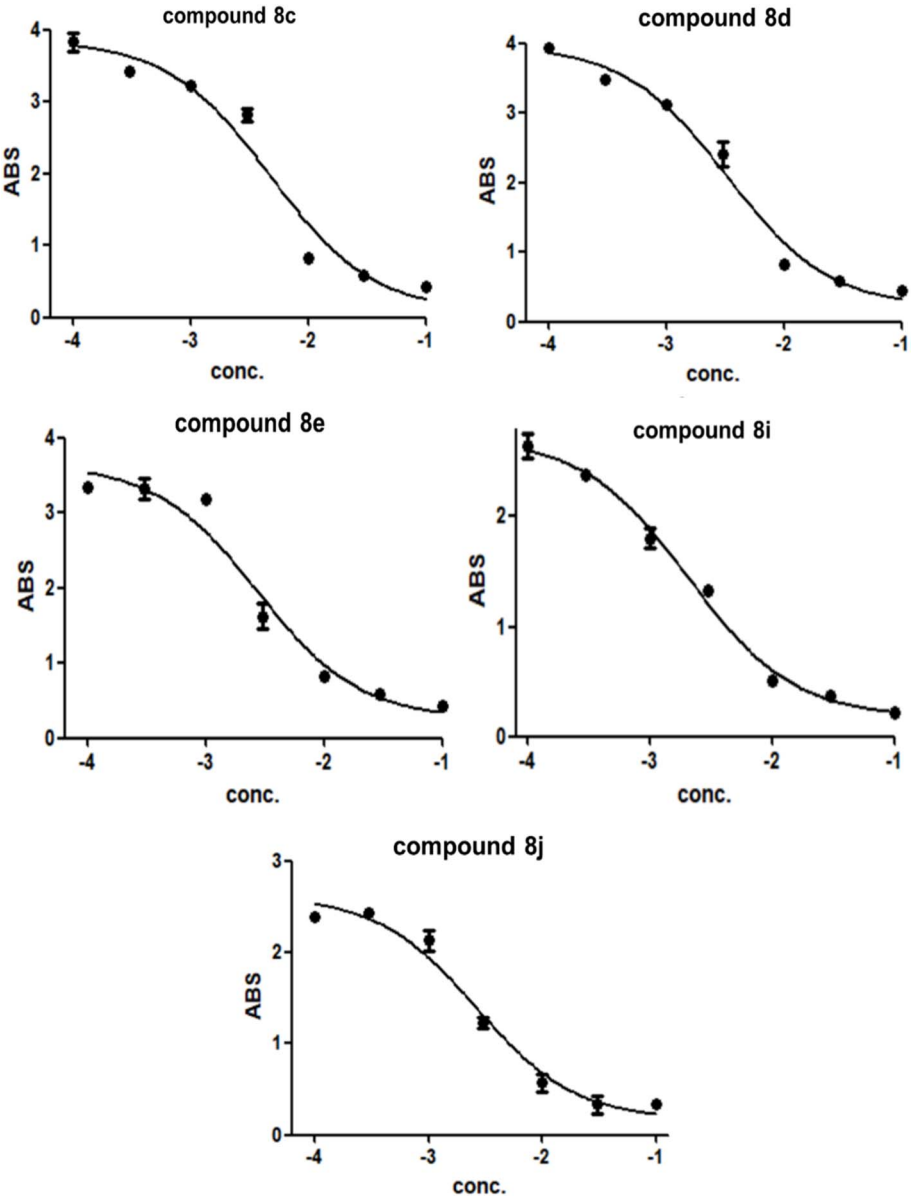

Fig. 8 Dose–response inhibition curves of compounds **8c**, **8d**, **8e**, **8i**, and **8j** against xanthine oxidase. The plots were generated by nonlinear regression of absorbance *versus* logarithmic concentration using GraphPad Prism. Results are presented as mean ± SEM ($n = 3$).

as dual enzyme inhibitors. These data indicate that the above conjugates represent promising scaffolds for the design of novel multifunctional agents with potential applications in the therapy of oxidative and neoplastic disorders.

The structure–activity relationships observed in this study can be rationalized in the context of the lophine–acylthiourea hybrid scaffold, in which the acylthiourea fragment functions as a privileged pharmacophore. Acylthiourea derivatives are well documented to exhibit strong enzyme-binding ability due to their dual hydrogen-bond donor–acceptor character and the presence of a thiocarbonyl sulfur capable of engaging in metal coordination and polar interactions. Comprehensive SAR analyses have demonstrated that such features significantly enhance binding affinity toward a wide range of enzyme targets, particularly metalloenzymes and phosphoryl-processing enzymes.[30]

The dose–response profiles shown in Fig. 8 and 9 reinforce the SAR that underpins the inhibitory behavior of the synthesized lophine-clubbed acylthiourea derivatives for xanthine oxidase, while compounds **8j**, **8i**, **8c**, and **8d** display steeper slopes with earlier inflection points, indicative of high-affinity binding and rapid achievement of maximal inhibition. The curve morphologies are in good agreement with the kinetic characteristics reported in the literature for several potent non-purine xanthine oxidase inhibitors, in which electron-withdrawing substituents and polymethoxy motifs are strongly associated with enhanced suppression of xanthine oxidase turnover.[54] For thymidine phosphorylase, the curves representing **8j**, **8d**, and **8a** reveal early saturation combined with a large

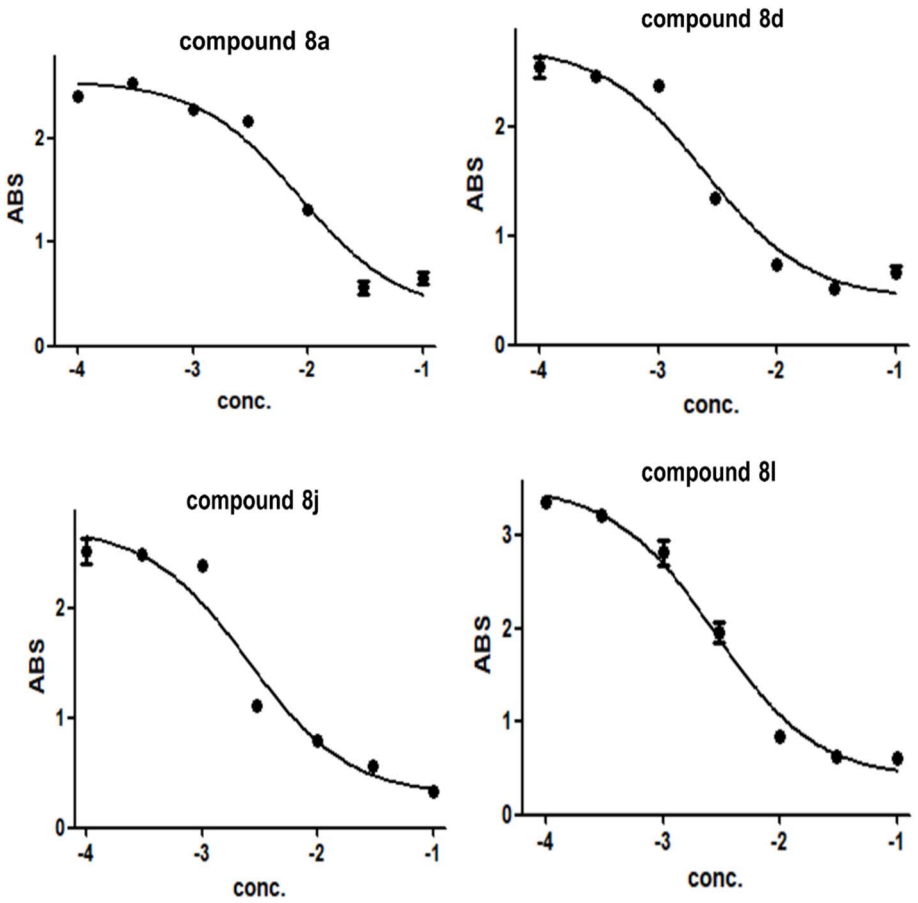

Fig. 9 Dose–response inhibition curves of compounds **8a**, **8d**, **8i**, and **8j** against thymidine phosphorylase. The plots were generated by nonlinear regression of absorbance *versus* logarithmic concentration using GraphPad Prism. Results are presented as mean ± SEM ($n = 3$).

magnitude of slopes, which points toward favorable aromatic alignment and high-affinity recognition in the narrower thymidine phosphorylase catalytic groove.[55]

The selectivity of enzyme inhibition by thiourea scaffolds has been a recurring theme in the field of medicinal chemistry. Thiourea and acylthiourea derivatives contribute unique structural features to a molecule, such as the presence of a thiocarbonyl functional group and NH groups that facilitate their use as both hydrogen bond donors and acceptors. This increases the degree of selectivity in the binding of enzymes to their ligands.[56] The sulfur atom in the thiocarbonyl group is also responsible for the formation of polar and electrostatic interactions that facilitate the binding of ligands in the active sites of enzymes. Due to these structural characteristics of the derivatives, thiourea derivatives have been widely evaluated as inhibitors of some important enzymes involved in biological processes and have been found to exhibit good binding selectivity in both biological assays and computational docking studies.[57,58] The presence of the acylthiourea linker in the synthesized lophine derivatives introduces a pharmacophore that is capable of making stable interactions with the residues of the catalytic pockets of both xanthine oxidase and thymidine phosphorylase enzymes, as evidenced by the inhibition trends observed in the biological assays.

2.3.1 Xanthine oxidase inhibition and SAR. To understand the SAR, we discuss the observed trends in terms of the electronic effects of the substituent groups, *i.e.*, whether the group is electron-withdrawing or electron-donating, as well as the steric effects, *i.e.*, the way the ligands are arranged around the enzyme's active site.

In vitro results on xanthine oxidase inhibition showed that electron-withdrawing substituents and polymethoxy substitution patterns substantially enhance activity. Electron-withdrawing groups have enhanced the inhibition of xanthine oxidase in this series of compounds. In compound **8j**, for example, the presence of the *meta*-nitro group makes this compound the most potent in the series, with an IC_{50} value of 1.87 μM. The electron-withdrawing ability of the nitro group increases the hydrogen-bond acceptor ability of the acylthiourea linker.[54]

The presence of electron-donating groups enhances activity in various derivatives. The presence of multiple methoxy groups in various derivatives, such as **8c** (3,5-di-OCH_3) and **8d** (3,4,5-tri-OCH_3), demonstrated robust xanthine oxidase inhibitory activity. The presence of methoxy groups enhances the aromatic polarizability and favors π–π stacking.[59]

Steric effects also seem to play a role in inhibitory activity. Inhibitors with *ortho*-substituted groups, such as **8e** and **8g**, demonstrated lower inhibitory activity. This lower inhibitory

activity may be due to steric effects that interfere with optimal ligand orientation and π-stacking.[54]

Compound **8i** (2-Cl,5-NO_2) is an example of the effect of halogens on inhibitory activity. The addition of chlorines generally enhances hydrophobic interactions within the binding pocket and extends the residence time of the compound. The nitro group is responsible for strong polar interactions with amino acids in the active site, which explains the potent xanthine oxidase inhibitory activity of this compound.[60] On the other hand, compounds with weakly polar or electronically neutral functional groups, such as **8a**, **8b**, and **8l**, displayed moderate xanthine oxidase inhibitory activity.

A comparison of their behavior from a side-by-side perspective illustrates a clear structure–activity relationship. The series demonstrates that electron-withdrawing groups, such as the *meta*-nitro group in **8j**, are the most potent inhibitors of xanthine oxidase activity. Compounds containing multiple methoxy groups (**8c** and **8d**) also outperform expectations, possibly because additional aromatic interactions within the binding site contribute to binding affinity. Conversely, compounds containing *ortho* groups (**8e** and **8g**) are less potent due to unfavorable steric interactions that prevent optimal binding orientation. In conclusion, the findings demonstrate the impact of both electronic and steric factors on the inhibitory activity of the lophine acylthiourea series.

2.3.2 Thymidine phosphorylase inhibition and SAR. In contrast to xanthine oxidase, thymidine phosphorylase has a more confined and rigid binding channel, which imposes stronger planarity requirements on the bound ligand. Thus, compound **8j** (3-NO_2) still shows the most potent thymidine phosphorylase inhibition, IC_{50} = 1.62 μM, since the dipolar nitro group exerts directional hydrogen-bonding interactions in the nucleoside recognition region. Although lophine-derived thymidine phosphorylase inhibitors have not been reported to date, a preliminary SAR study of thymidine phosphorylase in the heteroaryl–thiocarbonyl series indicated that nitro-substituted phenyl derivatives are often potent thymidine phosphorylase inhibitors, likely due to favorable dipolar alignment and charge complementarity.[61]

Compound **8d** (3,4,5-tri-OCH_3) is a very potent thymidine phosphorylase inhibitor (IC_{50} = 3.31 μM). The high density of methoxy substituents increases aromatic stacking with thymidine phosphorylase-binding residues and supports additional hydrogen bonding by oxygen lone pairs. Similar SAR trends have been observed for inhibitors containing a thiocarbonyl group, where aromatic rings containing multiple methoxy functional groups enhance the binding affinity within the catalytic pocket of the enzyme.[62]

Interestingly, compounds **8a** (H) and **8l** (3-CH_3) retain high thymidine phosphorylase activity without strong polar substituents. This is due to the persistence of molecular planarity and the fulfillment of the ideal hydrophobic fit of the lophine aromatic surface within the narrow thymidine phosphorylase channel. Similar results have been found in SAR studies of thymidine phosphorylase inhibitors, where flat aromatic rings are maintained if the central scaffold has enough hydrogen-bonding potential.[61]

In contrast, *ortho*-substituted compounds such as **8e** (2-CH_3), **8g** (2-Cl), and **8i** (2-Cl,5-NO_2) show reduced thymidine phosphorylase inhibition. This is because steric crowding at the *ortho* position invokes out-of-plane distortion of the benzamide phenyl ring, disrupting π-stacking and misaligning pharmacophoric atoms. Similar steric penalties associated with *ortho*-substitution have been consistently observed during SAR studies of thymidine phosphorylase inhibitors.[62]

Inspection of how these substituents influence the activity pattern of the synthesized compounds reveals a good relationship between structure and activity for inhibiting thymidine phosphorylase. The compounds bearing electron-withdrawing groups, such as the *meta*-nitro group of **8j**, demonstrated the most potent inhibitory activity on thymidine phosphorylase, which suggests favourable electrostatic interactions with the enzyme's active site. The compounds bearing multiple methoxy groups (**8d**) also demonstrated good inhibitory potential, likely due to increased opportunities for aromatic stacking interactions. The compounds bearing *ortho*-substituted groups, however, were less potent (**8e**, **8g**, **8i**), likely due to steric hindrance preventing optimal binding within the narrow thymidine phosphorylase channel.

A comparison of docking scores with experimental IC_{50} values reveals a clear trend: molecules with higher predicted binding energies, such as **8j** and **8d**, are generally more potent inhibitors *in vitro*. This supports the docking analysis as a valid explanation for the observed structure–activity relationship. Table 3 summarizes the key substituent effects observed in this set of compounds, highlighting the role of electron-withdrawing, electron-donating, and steric substituents on xanthine oxidase and thymidine phosphorylase inhibition.

Based on the SAR trends that we have observed, some design concepts can be proposed to further optimize the lophine–acylthiourea core structure. First, incorporating electron-withdrawing functional groups such as nitro substituents can improve binding affinity by enhancing electrostatic interactions. Second, the presence of multiple methoxy functional groups can facilitate in the facilitation of aromatic stacking interactions within the catalytic pocket of the enzyme. Third, it is best to avoid bulky substituents at the *ortho*-position due to steric clashes that can disrupt optimal ligand orientation.

From a pharmacology perspective, targeting xanthine oxidase and thymidine phosphorylase simultaneously may have potential advantages. Xanthine oxidase inhibitors have been employed in the treatment of hyperuricemia and gout because the inhibition of the enzyme reduces the production of uric acid and oxidative stress associated with various metabolic syndromes.[63] In addition, thymidine phosphorylase has been identified as a significant enzyme in cancer because it is associated with the metabolism of nucleotides, which promotes cancer progression.[64,65] Therefore, compounds that can modulate both targets and are sufficiently small to access both binding sites have the potential of providing a dual therapeutic strategy that combines antioxidant and anti-angiogenic activities.

Although further pharmacokinetic and *in vivo* studies are required to fully explore this possibility, the potent enzyme inhibition and docking of compounds **8j** and **8d** suggest that the lophine–acylthiourea template has the potential for the

Table 3 Summary of SAR trends observed in the lophine–acylthiourea series

Substituent type	Compound	Xanthine oxidase activity	Thymidine phosphorylase activity	SAR trend
Electron-withdrawing (NO_2)	**8j**	Very strong (IC_{50} = 1.87 μM)	Very strong (IC_{50} = 1.62 μM)	Enhances electrostatic interactions and hydrogen bonding
Electron-donating (multi-OCH_3)	**8c, 8d**	Strong	Strong	Improves π-stacking and aromatic interactions
Halogen + nitro	**8i**	Strong	Moderate	Halogens enhance hydrophobic interactions
Neutral/weak	**8a, 8b, 8l**	Moderate	Moderate-good	Activity maintained by scaffold planarity
Ortho-substitution	**8e, 8g**	Weak	Weak	Steric hindrance disrupts ligand orientation

development of multifunctional agents. Collectively, the results have consistently highlighted compound **8j** as the most promising dual-target inhibitor among the synthesized compounds.

3 Materials and methods

3.1 Procedure and material

All reagents used were devoid of any purification and bought from Sigma-Aldrich. Synthetic reactions were carried out in a cleaned and oven-dried apparatus. Solvents were dried using appropriate methods before their use in reactions. The melting point of all the synthesized solid compounds was determined in open-end capillaries using the Stuart SMP3 melting point apparatus. All the synthesized compounds were characterized by IR spectroscopy using a Thermo Fischer FT-IR instrument and ^{1}H and ^{13}C-NMR spectroscopy using Bruker Advance 300 and 75 MHz, respectively. NMR spectra were recorded in deuterated solvents such as DMSO-d_6 and acetone-d_6 using tetramethylsilane (TMS) as reference. Chemical shift values were reported in delta (δ) ppm, and coupling constant (J) values were calculated in hertz (Hz). The progress of each reaction was monitored by TLC using pre-coated silica-gel plates (Merck F_{254}, 0.2 mm). Spots on TLC plates were visualized using UV light of 254 and 365 nm wavelength. Ninhydrin stain was used for confirmation of the amine functional group. Lassaigne's test was used for the detection of sulfur atoms in synthesized organic compounds.

3.2 General synthetic pathway for synthesis of lophine clubbed acylthiourea derivatives (8a–l)

Steps involved in the synthesis of lophine clubbed acylthiourea derivatives are given below.

3.2.1 Synthesis of 2-(4-nitrophenyl)-4,5-diphenyl-1*H*-imidazole (3). A mixture of benzil (4.76 mmol, 1 eq.), 4-NO_2-benzaldehyde (5.71 mmol, 1.2 eq.), and ammonium acetate (23.78 mmol, 5 eq.) in glacial acetic acid (50 ml) was stirred under reflux for 8 hours under a nitrogen atmosphere. The progress of the reaction was monitored by TLC. After completion of the reaction, the mixture was cooled to room temperature and poured onto crushed ice. This resulted in the formation of yellow precipitates. The yellow precipitates obtained were filtered and extensively washed with water and then dried under vacuum. Finally, the collected yellow precipitates were recrystallized from aqueous ethanol to afford a pure compound. The synthesis of 2-(4-nitrophenyl)-4,5-diphenyl-1*H*-imidazole (**3**) was confirmed by comparing its color and melting point with the literature. It is a dark yellow solid, and its melting point is 248–249 °C (*lit.* 250–251 °C).[66] The compound was obtained in an excellent yield of up to 90%.

3.2.2 Synthesis of 4-(4,5-diphenyl-1*H*-imidazol-2-yl) aniline (4). Zinc dust (8.79 mmol, 3 eq.) was added at intervals of 10 minutes to the ice-cold solution of 2-(4-nitrophenyl)-4,5-diphenyl-1*H*-imidazole (2.93 mmol, 1 eq.) (**3**) and conc. HCl (17.58 mmol, 6 eq.) in methanol (40 ml) at 0 °C. Stirring was carried out for 30 minutes at this temperature, and it was further continued for 6 more hours at room temperature. The progress of the reaction was monitored by TLC. After completion of the reaction, the reaction mixture was filtered to remove the unreacted zinc metal. The filtrate obtained was diluted with distilled water until white precipitates of the respective amine formed. Precipitates formed were filtered off, washed several times with water, and then vacuum dried. The product was recrystallized from ethanol to afford a pure compound. The synthesis of 4-(4,5-diphenyl-1*H*-imidazol-2-yl)aniline (**4**) was confirmed by comparing its color and melting point with the literature. It is a white solid and its melting point is 209–210 °C (*lit.* 211–212 °C).[39] Its synthesis was also confirmed from LC-MS (m/z): 311.1 (M^-). The compound was obtained in a good yield of up to 75%.

3.2.3 Synthesis of novel lophine clubbed acyl thioureas (8a–l). Differently substituted benzoic acids (**5a–l**) (1 eq.) and thionyl chloride (1.2 eq.) were refluxed in dry DCM (3 ml) for 4 hours under a nitrogen atmosphere in the presence of 3 drops of DMF as a catalyst to afford the respective acid chlorides (**6a–l**). After completion of the reaction, solvent and excess thionyl chloride were removed by purging nitrogen gas through the flask containing the reaction mixture. Solution of freshly prepared acid chloride in dry acetone (10 ml) was added dropwise to the stirred solution of potassium thiocyanate (1.2 eq.) in dry acetone (10 ml). The reaction mixture was refluxed with continuous stirring for 2 hours and then cooled down to room temperature. A solution of 4-(4,5-diphenyl-1*H*-imidazol-2-yl) aniline (1 eq.) (**4**) in anhydrous acetone (10 ml) was added dropwise to the resulting reaction mixture and then stirred under reflux conditions for 12 hours. After reaction completion,

the mixture was cooled to room temperature and diluted with distilled water, which resulted in the formation of precipitates. The precipitates formed were filtered off, washed with distilled water, and then purified by trituration with acetone.

3.3 *In silico* studies

Xanthine oxidase and thymidine phosphorylase coordinates were acquired from the Protein Data Bank using PDB codes 3NRZ and 4EAD.[67,68] To determine whether the produced compounds might occupy the protein's active pocket in a fashion that would explain the enzyme's activity, a molecular docking investigation was carried out. 3D-structure of protein was downloaded from PDB and co-crystallized ligands and heteroatoms were removed. Then, molecular docking was performed by using the molecular operating environment (MOE) software.[69] The structure of synthesized compounds was carried out by ChemOffice 3D (2015), and optimization of energy was performed by Gaussian 09 by using the density functional theory and 6-311G basis set.[70] First, optimization of protein structure was performed by using the MOE software. Then, molecular docking was performed. Discovery visualizer (DSV) is used for the identification of 2D and 3D models for the docked compounds. The electrostatic and Lennard-Jones van der Waals interactions were found to be responsible for the retention in the active pocket. Each compound was given various poses because of the docking of compounds into the active pocket.

3.3.1 Thymidine phosphorylase inhibition assay. The synthesized compounds were evaluated for their inhibitory activity against thymidine phosphorylase using thymidine as a substrate. 7-Deazaxanthine served as the standard inhibitor, while wells without substrates were used as blanks. Absorbance measurements were recorded at 290 nm using a SpectraMax microplate reader (Molecular Devices, California, USA), following a standard protocol. The reaction mixture for thymidine phosphorylase inhibition assay consisted of 145 μL of potassium phosphate buffer (pH 7.4), 30 μL of thymidine phosphorylase, and 20 μL of thymidine substrate (1.5 mM, final concentration 0.5 mM), with a final reaction volume of 200 μL. Each well was supplemented with 5 μL of test compounds before incubation at 25 °C for 10 minutes. Absorbance was recorded at 10, 20, and 30 minutes. Thymidine phosphorylase inhibition was quantified in terms of IC_{50} values.[71]

3.3.2 Xanthine oxidase inhibition assay. The xanthine oxidase inhibition assay was performed using a slightly modified version of the prior study's methodology. Xanthine oxidase and xanthine stock solutions were made at concentrations of 1 U mL^{-1} and 50 mM, respectively. Allopurinol and all synthesized compounds were dissolved in DMSO (DMSO content <0.1%) to create stock solutions (100 mM). For three minutes, samples or blank PB buffer (100 μL) and enzyme solution (50 μL, 0.08 U mL^{-1}) were incubated at 37 °C. The reaction was then initiated by the addition of xanthine (50 μL, 0.48 mM, final concentration 0.5 mM) to a total reaction volume of 200 μL. A spectrophotometer (Thermo, USA) was used to scan the absorbance at 295 nm every 15 seconds for five minutes.[72] For every determination, three duplicates were carried out using allopurinol as the positive control.[73]

3.4 Experimental data

3.4.1 *N*-((4-(4,5-diphenyl-1*H*-imidazol-2-yl)phenyl) carbamothioyl)benzamide (8a).

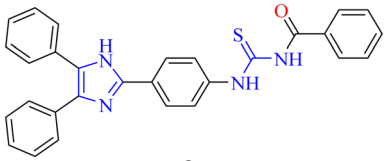

8a

White solid, m.p.: 228–229 °C, yield: 84%, R_f: 0.44 (*n*-hexane/EtOAc 7 : 3), FT-IR: $\bar{\nu}$ (cm^{-1}) 3215 (N–H), 3021 (Csp^2–H stretch), 1668 (C=O, carbonyl), 1594 (C=C, aromatic), 1259 (C=S), 1148 (C–N). ^{1}H-NMR: (300 MHz, DMSO-d_6): δ (ppm) 12.780 (s, 1H, NH), 11.660 (s, 1H, NH), 8.137 (d, ^3J = 8.4 Hz, 2H, Ar), 8.007 (d, ^3J = 7.5 Hz, 2H, Ar), 7.891 (d, ^3J = 8.4 Hz, 2H, Ar), 7.582–7.297 (m, 13H, Ar). ^{13}C-NMR: (75 MHz, DMSO-d_6): δ (ppm) 179.18 (C=S), 168.78 (C=O), 145.40 (C-imidazole), 138.48, 133.66, 133.17, 132.58, 129.19, 128.95, 128.28, 127.80, 126.04, 124.64 (C-aromatic). Anal. calcd. For $C_{29}H_{22}N_4OS$ (474.15): C, 73.39; N, 11.81; S, 6.76; H, 4.69% found: C, 73.37; N, 11.80; S7, 6.75; H, 4.66%.

3.4.2 *N*-((4-(4,5-diphenyl-1*H*-imidazol-2-yl)phenyl) carbamothioyl)-4-methyl benzamide (8b).

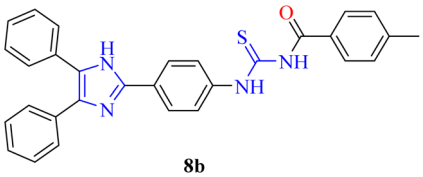

8b

Yellow solid, m.p.: 215–217 °C, yield: 78%, R_f: 0.45 (*n*-hexane/EtOAc 7 : 3), FT-IR: $\bar{\nu}$ (cm^{-1}) 3310 (N–H), 2971 (Csp^3–H), 1669 (C=O, carbonyl), 1590 (C=C, aromatic), 1260 (C=S), 1146 (C–N). ^{1}H-NMR: (300 MHz, DMSO-d_6): δ (ppm) 12.862 (s, 1H, NH), 11.598 (s, 1H, NH), 8.147 (d, ^3J = 8.7 Hz, 2H, Ar), 7.968–7.915 (m, 4H, Ar), 7.562–7.535 (m, 4H, Ar), 7.465–7.347 (m, 8H, Ar), 2.501 (s, 3H, aliphatic). ^{13}C-NMR: (75 MHz, DMSO-d_6): δ (ppm) 179.37 (C=S), 168.56 (C=O), 144.82 (C-imidazole), 144.23, 139.59, 131.90, 131.26, 129.54, 129.30, 129.15, 128.57, 126.80, 125.59, 124.69 (C-aromatic), 21.63 (C-methyl). Anal. calcd. For $C_{30}H_{24}N_4OS$ (488.17): C, 73.75; N, 11.47; S, 6.56; H, 4.95% found: C, 73.74; N, 11.46; S, 6.54; H, 4.94%.

3.4.3 *N*-((4-(4,5-diphenyl-1*H*-imidazol-2-yl)phenyl) carbamothioyl)-3,5-dimethoxybenzamide (8c).

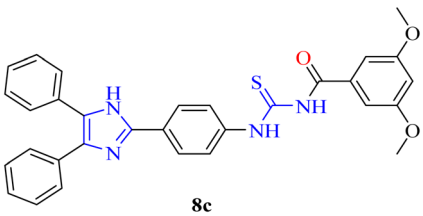

8c

Yellow solid, m.p.: 232–233 °C, yield: 74%, R_f: 0.35 (*n*-hexane/EtOAc 7 : 3), FT-IR: $\bar{\nu}$ (cm^{-1}) 3315 (N–H), 3001 (Csp^2–H), 1672 (C=O, carbonyl), 1589 (C=C, aromatic), 1207 (C=S), 1146 (C–N). ^{1}H-NMR: (300 MHz, DMSO-d_6): δ (ppm) 12.806 (s, 1H, NH),

11.679 (s, 1H, NH), 8.244 (d, ^3J = 8.4 Hz, 2H, aromatic), 7.974 (d, ^3J = 8.7 Hz, 2H, aromatic), 7.580–7.549 (m, 4H, aromatic), 7.478–7.401 (m, 6H, aromatic), 7.189 (d, ^3J = 2.1 Hz, 2H, aromatic), 6.784 (t, ^3J = 2.1 Hz, 1H, aromatic), 3.838 (s, 6H, methyl). ^{13}C-NMR: (75 MHz, DMSO-d_6): δ (ppm) 179.25 (C=S), 168.03 (C=O), 160.73 (C-aromatic), 144.58 (C-imidazole), 140.01, 134.38, 131.40, 130.46, 129.18, 128.89, 128.77, 127.28, 124.60, 106.82, 105.93 (C-aromatic), 56.10 (C-methyl). Anal. calcd. For $C_{31}H_{26}N_4O_3S$ (534.17): C, 69.64; N, 10.48; S, 6.00; H, 4.90% found: C, 69.62; N, 10.47; S, 5.98; H, 4.89%.

3.4.4 *N*-((4-(4,5-diphenyl-1*H*-imidazol-2-yl)phenyl) carbamothioyl)-3,4,5-trimethoxybenzamide (8d).

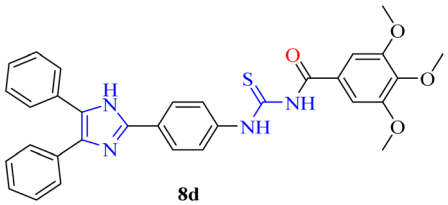

8d

Pale yellow solid, m.p.: 223–224 °C, yield: 78%, R_f: 0.25 (*n*-hexane/EtOAc 7 : 3), FT-IR: $\bar{\nu}$ (cm^{-1}) 3140 (N–H), 3031 (Csp^2–H), 2888 (Csp^3–H), 1680 (C=O, carbonyl), 1580 (C=C, aromatic), 1235 (C=S), 1118 (C–N). ^{1}H-NMR: (300 MHz, DMSO-d_6): δ (ppm) 12.971 (s, 1H, NH), 11.748 (s, 1H, NH), 8.373 (d, ^3J = 8.7 Hz, 2H, Ar), 8.057 (d, ^3J = 8.7 Hz, 2H, Ar), 7.599–7.569 (m, 6H, Ar), 7.492–7.471 (m, 4H, Ar), 7.413 (s, 2H, Ar), 3.889 (s, 6H, methyl), 3.761 (s, 3H, methyl). ^{13}C-NMR: (75 MHz, DMSO-d_6): δ (ppm) 179.49 (C=S), 167.69 (C=O), 143.89 (C-imidazole), 153.04, 142.13, 141.28, 130.05, 129.79, 129.35, 129.22, 128.38, 128.14, 127.04, 124.52, 121.52, 106.79 (C-aromatic), 60.64 (C-methyl), 56.63 (C-methyl). Anal. calcd. For $C_{32}H_{28}N_4O_4S$ (564.18): C, 68.07; N, 9.92; S, 5.68; H, 4.90% found: C, 68.06; N, 9.90; S, 5.67; H, 4.88%.

3.4.5 *N*-((4-(4,5-diphenyl-1*H*-imidazol-2-yl)phenyl) carbamothioyl)-2-methylbenzamide (8e).

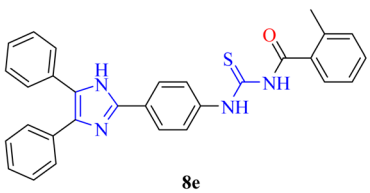

8e

Light orange solid, m.p.: 212–214 °C, yield: 83%, R_f: 0.61 (*n*-hexane/EtOAc 7 : 3), FT-IR: $\bar{\nu}$ (cm^{-1}) 3110 (N–H), 3010 (Csp^2–H), 2924 (Csp^3–H), 1674 (C=O, carbonyl), 1591 (C=C, aromatic), 1255 (C=S), 1148 (C–N). ^{1}H-NMR: (300 MHz, acetone-d_6): δ (ppm) 13.098 (s, 1H, NH), 10.647 (s, 1H, NH), 8.400 (d, ^3J = 8.7 Hz, 2H, Ar), 8.177 (d, ^3J = 8.7 Hz, 2H, Ar), 7.666–7.617 (m, 5H, Ar), 7.513–7.452 (m, 7H, Ar), 7.374–7.348 (m, 2H, Ar), 2.537 (s, 3H, methyl). ^{13}C-NMR: (75 MHz, acetone-d_6): δ (ppm) 178.78 (C=S), 170.71 (C=O), 144.15 (C-imidazole), 141.18, 136.93, 134.23, 133.66, 131.45, 131.07, 130.06, 129.28, 128.87, 128.79, 128.04, 127.94, 127.85, 125.77, 123.52, 123.37, 121.12 (C-aromatic), 19.15 (C-methyl). Anal. calcd. For $C_{30}H_{24}N_4OS$ (488.17): C, 73.75; N, 11.47; S, 6.56; H, 4.95% found: C, 73.74; N, 11.46; S, 6.54; H, 4.93%.

3.4.6 *N*-((4-(4,5-diphenyl-1*H*-imidazol-2-yl)phenyl) carbamothioyl)-4-nitrobenzamide (8f).

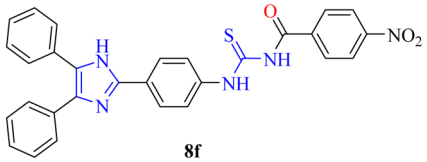

8f

Dark orange solid, m.p.: 204–206 °C, yield: 75%, R_f: 0.55 (*n*-hexane/EtOAc 7 : 3), FT-IR: $\bar{\nu}$ (cm^{-1}) 3110 (N–H), 3037 (Csp^2–H), 1675 (C=O, carbonyl), 1587 (C=C, aromatic), 1261 (C=S), 1314 and 1529 (NO_2), 1130 (C–N). Anal. calcd. For $C_{29}H_{21}N_5O_3S$ (519.14): C, 67.04; N, 13.48; S, 6.17; H, 4.07% found: C, 67.02; N, 13.49; S, 6.16; H, 4.06%.

3.4.7 2-Chloro-*N*-((4-(4,5-diphenyl-1*H*-imidazol-2-yl) phenyl)carbamothioyl)benzamide (8g).

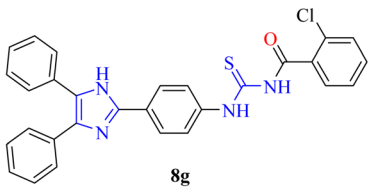

8g

Dark orange solid, m.p.: 185–187 °C, yield: 80%, R_f: 0.41 (*n*-hexane/EtOAc 7 : 3), FT-IR: $\bar{\nu}$ (cm^{-1}) 3125 (N–H), 3017 (Csp^2–H), 1677 (C=O, carbonyl), 1585 (C=C, aromatic), 1259 (C=S), 1151 (C–N). Anal. calcd. For $C_{29}H_{21}ClN_4OS$ (508.11): C, 68.43; N, 11.01; S, 6.30; H, 4.16% found: C, 68.42; N, 11.00; S, 6.32; H, 4.14%.

3.4.8 *N*-((4-(4,5-diphenyl-1*H*-imidazol-2-yl)phenyl) carbamothioyl)-4-methoxybenzamide (8h).

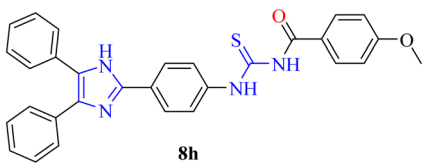

8h

Dark orange solid, m.p.: 230–231 °C, yield: 85%, R_f: 0.35 (*n*-hexane/EtOAc 7 : 3), FT-IR: $\bar{\nu}$ (cm^{-1}) 3305 (N–H), 3026 (Csp^2–H), 1648 (C=O, carbonyl), 1591 (C=C, aromatic), 1256 (C=S), 1147 (C–N). Anal. calcd. For $C_{30}H_{24}N_4O_2S$ (504.16): C, 71.41; N, 11.10; S, 6.35; H, 4.79% found: C, 71.39; N, 11.11; S, 6.35; H, 4.78%.

3.4.9 2-Chloro-*N*-((4-(4,5-diphenyl-1*H*-imidazol-2-yl) phenyl)carbamothioyl)-5-nitrobenzamide (8i).

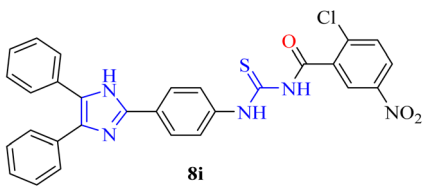

8i

Pale yellow solid, m.p.: 275–277 °C, yield: 70%, R_f: 0.55 (*n*-hexane/EtOAc 7 : 3), FT-IR: $\bar{\nu}$ (cm^{-1}) 3128 (N–H), 3033 (Csp^2–H), 2893 (Csp^3–H), 1681 (C=O, carbonyl), 1580 (C=C,

aromatic), 1235 (C=S), 1108 (C–N). Anal. calcd. For $C_{29}H_{20}ClN_5O_3S$ (553.10): C, 62.87; N, 12.64; S, 5.79; H, 3.64% found: C, 62.85; N, 12.63; S, 5.80; H, 3.63%.

3.4.10 *N*-((4-(4,5-diphenyl-1*H*-imidazol-2-yl)phenyl) carbamothioyl)-3-nitrobenzamide (8j).

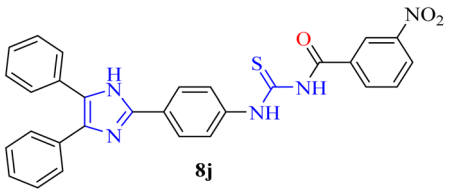

8j

White solid, m.p.: 215–217 °C, yield: 72%, R_f: 0.21 (*n*-hexane/EtOAc 7 : 3), FT-IR: $\bar{\nu}$ (cm^{-1}) 3301 (N–H), 2995 (Csp^2–H), 2863 (Csp^3–H), 1644 (C=O, carbonyl), 1600 (C=C, aromatic), 1253 (C=S), 1128 (C–N). Anal. calcd. For $C_{29}H_{21}N_5O_3S$ (519.14): C, 67.04; N, 13.48; S, 6.17; H, 4.07% found: C, 67.03; N, 13.47; S, 6.15; H, 4.08%.

3.4.11 4-Chloro-*N*-((4-(4,5-diphenyl-1*H*-imidazol-2-yl) phenyl)carbamothioyl)benzamide (8k).

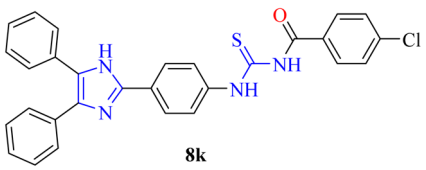

8k

Beige color solid, m.p.: 237–238 °C, yield: 70%, R_f: 0.55 (*n*-hexane/EtOAc 7 : 3), FT-IR: $\bar{\nu}$ (cm^{-1}) 3118 (N–H), 3052 (Csp^2–H), 1646 (C=O, carbonyl), 1588 (C=C, aromatic), 12 338 (C=S), 1089 (C–N). Anal. calcd. For $C_{29}H_{21}ClN_4OS$ (508.11): C, 68.43; N, 11.01; S, 6.30; H, 4.16% found: C, 68.41; N, 11.00; S, 6.31; H, 4.15%.

3.4.12 *N*-((4-(4,5-diphenyl-1*H*-imidazol-2-yl)phenyl) carbamothioyl)-3-methylbenzamide 8l.

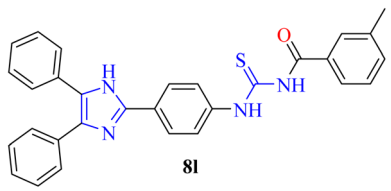

8l

Orange solid, m.p.: 230–232 °C, yield: 74%, R_f: 0.37 (*n*-hexane/EtOAc 7 : 3), FT-IR: $\bar{\nu}$ (cm^{-1}) 3106 (N–H), 3049 (Csp^2–H), 2833 (Csp^3–H), 1669 (C=O, carbonyl), 1598 (C=C, aromatic), 1254 (C=S), 1188 (C–N). Anal. calcd. For $C_{30}H_{24}N_4OS$ (488.17): C, 73.75; N, 11.47; S, 6.56; H, 4.95% found: C, 73.74; N, 11.45; S, 6.57; H, 4.94%.

4 Conclusion

A facile multistep synthesis of lophine clubbed acylthiourea derivatives is reported in this study involving heterocyclization, reduction, nucleophilic substitution, and addition reactions. In view of their relevance to advanced medicinal chemistry, the compounds were synthesized using straightforward procedures that avoided harsh conditions and minimized purification requirements. Beyond synthetic convenience, the lophine–acylthiourea derivatives were found to exert significant *in vitro* dual inhibition of xanthine oxidase and thymidine phosphorylase. Indeed, within this series, the analogs **8j**, **8d**, and **8i** displayed very potent activity, with IC_{50} values in the low micromolar range. Molecular docking studies further supported these findings, as they indicated the binding interactions of the active compounds with the catalytic sites of both enzymes were favorable, and their accommodation was stable. The close agreement between *in vitro* results and computational predictions underlined the potential of this compound series as a versatile scaffold for modulating both oxidative stress and purine metabolism. Overall, the results provide a solid basis for future studies focusing on the rational design and development of dual-target enzyme inhibitors with therapeutic relevance.

Conflicts of interest

There are no conflicts to declare.

Data availability

The manuscript includes all relevant data which was generated or analyzed during this study. Additional information is included in the supplementary information (SI). Supplementary information: spectroscopic characterization data. See DOI: https://doi.org/10.1039/d6ra01337f.

References

1 C. Viegas-Junior, A. Danuello, V. da Silva Bolzani, E. J. Barreiro and C. A. M. Fraga, Molecular hybridization: a useful tool in the design of new drug prototypes, *Curr. Med. Chem.*, 2007, **14**, 1829–1852.
2 A. Bhatnagar, P. Sharma and N. Kumar, A review on "Imidazoles": Their chemistry and pharmacological potentials, *Int. J. PharmTech Res.*, 2011, **3**, 268–282.
3 A. Gueiffier, S. Mavel, M. Lhassani, A. Elhakmaoui, R. Snoeck, G. Andrei, O. Chavignon, J.-C. Teulade, M. Witvrouw and J. Balzarini, Synthesis of imidazo [1, 2-a] pyridines as antiviral agents, *J. Med. Chem.*, 1998, **41**, 5108–5112.
4 S. Y. Atanasova-Stamova, S. F. Georgieva and M. B. Georgieva, Reaction strategies for synthesis of imidazole derivatives: a review, *Scr. Sci. Pharm.*, 2018, **5**, 7–13.
5 R. A. Hill, Marine natural products, *Annu. Rep. Prog. Chem., Sect. B:Org. Chem.*, 2009, **105**, 150–166.
6 B. Forte, B. Malgesini, C. Piutti, F. Quartieri, A. Scolaro and G. Papeo, A submarine journey: The pyrrole-imidazole alkaloids, *Mar. Drugs*, 2009, **7**, 705–753.
7 Z. Jin, Muscarine, imidaozle, oxazole and thiazole alkaloids, *Nat. Prod. Rep.*, 2013, **30**, 869–915.
8 G. Gao, R. Xiao, Y. Yuan, C.-H. Zhou, J. You and R.-G. Xie, Efficient imidazolium catalysts for the benzoin condensation, *J. Chem. Res.*, 2002, **2002**, 262–263.

9 H.-Y. Jiang, C.-H. Zhou, K. Luo, H. Chen, J.-B. Lan and R.-G. Xie, Chiral imidazole metalloenzyme models: Synthesis and enantioselective hydrolysis for α-amino acid esters, *J. Mol. Catal. A: Chem.*, 2006, **260**, 288–294.
10 H. V. Tolomeu and C. A. M. Fraga, Imidazole: synthesis, functionalization and physicochemical properties of a privileged structure in medicinal chemistry, *Molecules*, 2023, **28**, 838.
11 V. R. Pattabiraman and J. W. Bode, Rethinking amide bond synthesis, *Nature*, 2011, **480**, 471–479.
12 K. Liaras, A. Geronikaki, J. Glamočlija, A. Ćirić and M. Soković, Thiazole-based chalcones as potent antimicrobial agents. Synthesis and biological evaluation, *Bioorg. Med. Chem.*, 2011, **19**, 3135–3140.
13 X. Lu, X. Liu, B. Wan, S. G. Franzblau, L. Chen, C. Zhou and Q. You, Synthesis and evaluation of anti-tubercular and antibacterial activities of new 4-(2, 6-dichlorobenzyloxy) phenyl thiazole, oxazole and imidazole derivatives. Part 2, *Eur. J. Med. Chem.*, 2012, **49**, 164–171.
14 D. Varadaraji, S. S. Suban, V. R. Ramasamy, K. Kubendiran, J. S. K. Raguraman, S. K. Nalilu and H. N. Pati, Synthesis and evaluation of a series of 1-substituted tetrazole derivatives as antimicrobial agents, *Org. Commun.*, 2010, **3**, 45–56.
15 F. K. Keter and J. Darkwa, Perspective: the potential of pyrazole-based compounds in medicine, *BioMetals*, 2012, **25**, 9–21.
16 C.-H. Zhou and Y. Wang, Recent researches in triazole compounds as medicinal drugs, *Curr. Med. Chem.*, 2012, **19**, 239–280.
17 L. Zhang, X. M. Peng, G. L. Damu, R. X. Geng and C. H. Zhou, Comprehensive review in current developments of imidazole-based medicinal chemistry, *Med. Res. Rev.*, 2014, **34**, 340–437.
18 B. Radziszewski, Untersuchungen über hydrobenzamid, amarin und lophin, *Ber. Dtsch. Chem. Ges.*, 1877, **10**, 70–75.
19 R. Gandhaveeti, R. Konakanchi, P. Jyothi, N. S. Bhuvanesh and S. Anandaram, Unusual coordination mode of aroyl/acyl thiourea ligands and their π-arene ruthenium (II) piano-stool complexes: Synthesis, molecular geometry, theoretical studies and biological applications, *Appl. Organomet. Chem.*, 2019, **33**, 4899.
20 F. Salomon, Ueber die Schwefelkohlensäureäther, *J. Prakt. Chem.*, 1873, (6), 433–453.
21 D. C. Schroeder, Thioureas, *Chem. Rev.*, 1955, **55**, 181–228.
22 Z.-n. Wang, H. Zhong, S. Wang, G.-y. Liu and Q. Zhang, Synthesis of 1, 4-benzenedicarbonyl thiourea resins and their adsorption properties for Ag (I), *J. Cent. South Univ.*, 2011, **18**, 361–366.
23 Y. Nural, E. Karasu, E. Keleş, B. Aydıner, N. Seferoğlu, Ç. Efeoğlu, E. Şahin and Z. Seferoğlu, Synthesis of novel acylthioureas bearing naphthoquinone moiety as dual sensor for high-performance naked-eye colorimetric and fluorescence detection of CN− and F− ions and its application in water and food samples, *Dyes Pigm.*, 2022, **198**, 110006.
24 E. M. Hoshall, Report on Preservatives and Artificial Sweeteners, *J. Assoc. Off. Agric. Chem.*, 1964, **47**, 68.
25 W. T. Lambert, M. E. Goldsmith and T. C. Sparks, Insecticidal activity of novel thioureas and isothioureas, *Pest Manage. Sci.*, 2017, **73**, 743–751.
26 I. L. Goncalves, G. O. de Azambuja, D. F. Kawano and V. L. Eifler-Lima, Thioureas as building blocks for the generation of heterocycles and compounds with pharmacological activity: An overview, *Mini-Rev. Org. Chem.*, 2018, **15**, 28–35.
27 M. K. Rauf, A. Badshah, M. Gielen, M. Ebihara, D. de Vos and S. Ahmed, Synthesis, structural characterization and in vitro cytotoxicity and anti-bacterial activity of some copper (I) complexes with N, N′-disubstituted thioureas, *J. Inorg. Biochem.*, 2009, **103**, 1135–1144.
28 J. M. Andrés, A. Maestro, M. Valle and R. Pedrosa, Chiral Bifunctional Thioureas and Squaramides and Their Copolymers as Recoverable Organocatalysts. Stereoselective Synthesis of 2-Substituted 4-Amino-3-nitrobenzopyrans and 3-Functionalized 3, 4-Diamino-4 H-Chromenes, *J. Org. Chem.*, 2018, **83**, 5546–5557.
29 T. Parvin, R. Yadav and L. H. Choudhury, Recent applications of thiourea-based organocatalysts in asymmetric multicomponent reactions (AMCRs), *Org. Biomol. Chem.*, 2020, **18**, 5513–5532.
30 S. A. Ullah, A. Saeed, M. Azeem, M. B. Haider and M. F. Erben, Exploring the latest trends in chemistry, structure, coordination, and diverse applications of 1-acyl-3-substituted thioureas: a comprehensive review, *RSC Adv.*, 2024, **14**, 18011–18063.
31 A. Maalik, H. Rahim, M. Saleem, N. Fatima, A. Rauf, A. Wadood, M. I. Malik, A. Ahmed, H. Rafique and M. N. Zafar, Synthesis, antimicrobial, antioxidant, cytotoxic, antiurease and molecular docking studies of N-(3-trifluoromethyl) benzoyl-N′-aryl thiourea derivatives, *Bioorg. Chem.*, 2019, **88**, 102946.
32 M. Khan, J. Patujo, I. Mushtaq, A. Ishtiaq, M. N. Tahir, S. Bibi, M. S. Khan, G. Mustafa, B. Mirza and A. Badshah, Anti-diabetic potential, crystal structure, molecular docking, DFT, and optical-electrochemical studies of new dimethyl and diethyl carbamoyl-N, N′-disubstituted based thioureas, *J. Mol. Struct.*, 2022, **1253**, 132207.
33 J.-h. Li, Y. Wang, Y.-p. Wu, R.-h. Li, S. Liang, J. Zhang, Y.-g. Zhu and B.-j. Xie, Synthesis, herbicidal activity study and molecular docking of novel pyrimidine thiourea, *Pestic. Biochem. Physiol.*, 2021, **172**, 104766.
34 H. Wang, Z.-W. Zhai, Y.-X. Shi, C.-X. Tan, J.-Q. Weng, L. Han, B.-J. Li and X.-H. Liu, Novel trifluoromethylpyrazole acyl thiourea derivatives: synthesis, antifungal activity and docking study, *Lett. Drug Des. Discovery*, 2019, **16**, 785–791.
35 G. M. Viana, D. C. Soares, M. V. Santana, L. H. do Amaral, P. W. Meireles, R. P. Nunes, L. C. R. P. da Silva, L. C. de Sequeira Aguiar, C. R. Rodrigues and V. P. de Sousa, Antileishmanial thioureas: synthesis, biological activity and in silico evaluations of new promising derivatives, *Chem. Pharm. Bull.*, 2017, **65**, 911–919.
36 M. Irani, K. R. Ranjbar and H. Izadi, *The Synthesis of Some New Benzoyl Thioureas and Investigation of Pesticide Activity*, 2014.

37 T. A. Fattah, A. Saeed, Z. Ashraf, Q. Abbas, P. A. Channar, F. A. Larik and M. Hassan, 4-Aminocoumarin based aroylthioureas as potential jack bean urease inhibitors; synthesis, enzyme inhibitory kinetics and docking studies, *Med. Chem.*, 2020, **16**, 229–243.

38 İ. Koca, A. Özgür, K. A. Coşkun and Y. Tutar, Synthesis and anticancer activity of acyl thioureas bearing pyrazole moiety, *Bioorg. Med. Chem.*, 2013, **21**, 3859–3865.

39 P. Reigan, A. Gbaj, I. J. Stratford, R. A. Bryce and S. Freeman, Xanthine oxidase-activated prodrugs of thymidine phosphorylase inhibitors, *Eur. J. Med. Chem.*, 2008, **43**, 1248–1260.

40 S. Kalra, G. Jena, K. Tikoo and A. K. Mukhopadhyay, Preferential inhibition of xanthine oxidase by 2-amino-6-hydroxy-8-mercaptopurine and 2-amino-6-purine thiol, *BMC Biochem.*, 2007, **8**, 8.

41 S. Prachayasittikul, R. Pingaew, A. Worachartcheewan, N. Sinthupoom, V. Prachayasittikul, S. Ruchirawat and V. Prachayasittikul, Roles of pyridine and pyrimidine derivatives as privileged scaffolds in anticancer agents, *Mini-Rev. Med. Chem.*, 2017, **17**, 869–901.

42 L.-X. Zhao, K. Luo, X.-D. Guo, Y.-L. Zou, S. Gao, Y. Fu and F. Ye, Design, Synthesis, and Biological Activity Evaluation of Novel Phenoxypyridine Derivatives Containing Acylthiourea Fragments as Protoporphyrinogen Oxidase Inhibitor Herbicides, *J. Agric. Food Chem.*, 2025, **73**, 5020–5032.

43 K. Okamoto, B. T. Eger, T. Nishino, E. F. Pai and T. Nishino, Mechanism of inhibition of xanthine oxidoreductase by allopurinol: crystal structure of reduced bovine milk xanthine oxidoreductase bound with oxipurinol, *Nucleosides, Nucleotides Nucleic Acids*, 2008, **27**, 888–893.

44 H. Xue, M. Xu, D. Gong and G. Zhang, Mechanism of flavonoids inhibiting xanthine oxidase and alleviating hyperuricemia from structure–activity relationship and animal experiments: A review, *Food Front.*, 2023, **4**, 1643–1665.

45 A. Mehmood, J. Li, A. U. Rehman, R. Kobun, I. U. Llah, I. Khan, F. Althobaiti, S. Albogami, M. Usman, F. Alharthi, M. M. Soliman, S. Yaqoob, K. A. Awan, L. Zhao and L. Zhao, Xanthine oxidase inhibitory study of eight structurally diverse phenolic compounds, *Front. Nutr.*, 2022, **9**, 966557.

46 J. Chen, Z. He, S. Yu, X. Cai, D. Zhu and Y. Lin, Xanthine oxidase inhibitory kinetics and mechanism of ellagic acid: In vitro, in silico and in vivo studies, *IET Nanobiotechnol.*, 2023, **17**, 368–375.

47 Q. Feng, W. Yang, Z. Peng and G. Wang, Recent advances in the synthetic thymidine phosphorylase inhibitors for cancer therapy, *Eur. J. Pharmacol.*, 2022, **934**, 175319.

48 M. F. S. de Abreu, C. A. Wegermann, M. S. Ceroullo, I. G. M. Sant'Anna and R. C. S. Lessa, Ten Years Milestones in Xanthine Oxidase Inhibitors Discovery: Febuxostat-Based Inhibitors Trends, Bifunctional Derivatives, and Automatized Screening Assays, *Organics*, 2022, **3**, 380–414.

49 A. Gul, S. M. Saad, H. Zafar, W. Atia Tul, K. M. Khan and M. I. Choudhary, In vitro and In silico Xanthine Oxidase Inhibitory Activities of 3-Aryl-2- thioxo-2,3-dihydroquinazolin-4(1H)-one Derivatives, *Med. Chem.*, 2023, **19**, 384–392.

50 O. L. Kobzar, I. M. Mischenko, A. V. Tatarchuk, V. S. Vdovin, S. S. Lukashov, S. M. Yarmoluk and A. I. Vovk, Nitro-substituted aurones as xanthine oxidase inhibitors, *Ukr. Bioorg. Acta*, 2021, **16**, 12–17.

51 M. A. Sajid, Z. A. Khan, S. A. Shahzad, S. A. R. Naqvi, M. Usman and A. Iqbal, Recent advances in thymidine phosphorylase inhibitors: Syntheses and prospective medicinal applications, *Turk. J. Chem.*, 2017, **41**, 1–28.

52 K. Zaman, F. Rahim, M. Taha, A. Wadood, S. A. A. Shah, Q. U. Ahmed and Z. A. Zakaria, Synthesis of new isoquinoline-base-oxadiazole derivatives as potent inhibitors of thymidine phosphorylase and molecular docking study, *Sci. Rep.*, 2019, **9**, 16015.

53 R. Hussain, W. Rehman, F. Rahim, S. Khan, A. S. Alanazi, M. M. Alanazi, L. Rasheed, Y. Khan, S. A. A. Shah and M. Taha, Synthesis, in vitro thymidine phosphorylase inhibitory activity and molecular docking study of novel pyridine-derived bis-oxadiazole bearing bis-schiff base derivatives, *Arabian J. Chem.*, 2023, **16**, 104773.

54 N. Zhai, C. Wang, F. Wu, L. Xiong, X. Luo, X. Ju and G. Liu, Exploration of Novel Xanthine Oxidase Inhibitors Based on 1,6-Dihydropyrimidine-5-Carboxylic Acids by an Integrated in Silico Study, *Int. J. Mol. Sci.*, 2021, **22**, 8122.

55 T. M. Cui, M. Altaf, A. Aldarhami, A. S. Bazaid, N. H. Saeedi, A. A. Alkayyal, F. M. Alshabrmi, F. Ali, M. Aladhadh, M. Y. Khan, A. A. Alsaiari and Y. R. Ma, Dihydropyrimidone Derivatives as Thymidine Phosphorylase Inhibitors: Inhibition Kinetics, Cytotoxicity, and Molecular Docking, *Molecules*, 2023, **28**, 3634.

56 H. Zaman, A. Saeed, H. Ismail and M. Rashid, Unveiling the cyclopropyl appended acyl thiourea derivatives as antimicrobial, α-amylase and proteinase K inhibitors: Design, synthesis, biological evaluation, molecular docking, DFT and ADMET studies, *Arch. Biochem. Biophys.*, 2025, **765**, 110304.

57 F. U. Rahman, M. Bibi, E. Khan, A. B. Shah, M. Muhammad, M. N. Tahir, A. Shahzad, F. Ullah, M. Zahoor, S. Alamery and G. E. Batiha, Thiourea Derivatives, Simple in Structure but Efficient Enzyme Inhibitors and Mercury Sensors, *Molecules*, 2021, **26**, 4506.

58 R. Ronchetti, G. Moroni, A. Carotti, A. Gioiello and E. Camaioni, Recent advances in urea- and thiourea-containing compounds: focus on innovative approaches in medicinal chemistry and organic synthesis, *RSC Med. Chem.*, 2021, **12**, 1046–1064.

59 E. Noriega-Iribe, L. Díaz-Rubio, A. Estolano-Cobián, V. W. Barajas-Carrillo, J. M. Padrón, R. Salazar-Aranda, R. Díaz-Molina, V. García-González, R. A. Chávez-Santoscoy, D. Chávez and I. Córdova-Guerrero, In Vitro and In Silico Screening of 2,4,5-Trisubstituted Imidazole Derivatives as Potential Xanthine Oxidase and

Acetylcholinesterase Inhibitors, Antioxidant, and Antiproliferative Agents, *Appl. Sci.*, 2020, **10**, 2889.

60 N. Arshad, U. Parveen, P. A. Channar, A. Saeed, W. S. Saeed, F. Perveen, A. Javed, H. Ismail, M. I. Mir, A. Ahmed, B. Azad and I. Khan, Investigation of Newly Synthesized Bis-Acyl-Thiourea Derivatives of 4-Nitrobenzene-1,2-Diamine for Their DNA Binding, Urease Inhibition, and Anti-Brain-Tumor Activities, *Molecules*, 2023, **28**, 2707.

61 T. Glomb, K. Szymankiewicz and P. Świątek, Anti-Cancer Activity of Derivatives of 1,3,4-Oxadiazole, *Molecules*, 2018, **23**, 3361.

62 A. Murmu, P. Banjare, B. W. Matore, P. P. Roy and J. Singh, 1, 3, 4-Oxadiazole: an emerging scaffold to inhibit the thymidine phosphorylase as an anticancer agent, *Curr. Med. Chem.*, 2024, **31**, 6227–6250.

63 T. Nishikawa, N. Nagata, T. Shimakami, T. Shirakura, C. Matsui, Y. Ni, F. Zhuge, L. Xu, G. Chen, M. Nagashimada, T. Yamashita, Y. Sakai, T. Yamashita, E. Mizukoshi, M. Honda, S. Kaneko and T. Ota, Xanthine oxidase inhibition attenuates insulin resistance and diet-induced steatohepatitis in mice, *Sci. Rep.*, 2020, **10**, 815.

64 B. Huang, Q. Yuan, J. Sun, C. Wang and D. Yang, Thymidine phosphorylase in nucleotide metabolism: physiological functions and its implications in tumorigenesis and anti-cancer therapy, *Front. Immunol.*, 2025, **16**, 1561560.

65 T. Furukawa, S. Tabata, M. Yamamoto, K. Kawahara, Y. Shinsato, K. Minami, M. Shimokawa and S.-i. Akiyama, Thymidine phosphorylase in cancer aggressiveness and chemoresistance, *Pharmacol. Res.*, 2018, **132**, 15–20.

66 A. Puratchikody, M. Nallu and S. Gopalakrishnan, Synthesis and Pharmacological Evaluation of Some Potent 2-(4-Substitutedphenyl)-4,5-Diphenyl-1*H*-Imidazoles, *Indian J. Pharm. Sci.*, 2005, **67**, 725–731.

67 S. A. Shahzad, M. Yar, Z. A. Khan, L. Shahzadi, S. A. R. Naqvi, A. Mahmood, S. Ullah, A. J. Shaikh, T. A. Sherazi and A. T. Bale, Identification of 1, 2, 4-triazoles as new thymidine phosphorylase inhibitors: Future anti-tumor drugs, *Bioorg. Chem.*, 2019, **85**, 209–220.

68 S. Chakravarty and K. Kannan, Drug-protein interactions: refined structures of three sulfonamide drug complexes of human carbonic anhydrase I enzyme, *J. Mol. Biol.*, 1994, **243**, 298–309.

69 S. Vilar, G. Cozza and S. Moro, Medicinal chemistry and the molecular operating environment (MOE): application of QSAR and molecular docking to drug discovery, *Curr. Top. Med. Chem.*, 2008, **8**, 1555–1572.

70 A. Frisch, *Gaussian 09W Reference*, Wallingford, USA, 2009, vol. 470, p. , p. 25.

71 S. A. Shahzad, M. Yar, M. Bajda, L. Shahzadi, Z. A. Khan, S. A. R. Naqvi, S. Mutahir, N. Mahmood and K. M. Khan, Synthesis, thymidine phosphorylase inhibition and molecular modeling studies of 1, 3, 4-oxadiazole-2-thione derivatives, *Bioorg. Chem.*, 2015, **60**, 37–41.

72 D. A. Kostić, D. S. Dimitrijević, G. S. Stojanović, I. R. Palić, A. S. Đorđević and J. D. Ickovski, Xanthine oxidase: isolation, assays of activity, and inhibition, *J. Chem.*, 2015, 294858.

73 J. Zhao, L. Huang, C. Sun, D. Zhao and H. Tang, Studies on the structure-activity relationship and interaction mechanism of flavonoids and xanthine oxidase through enzyme kinetics, spectroscopy methods and molecular simulations, *Food Chem.*, 2020, **323**, 126807.